REPORT DOCUMENTATION PAGE		Form Approved OMB No. 0704-0188

Public reporting burden for this collection of information is estimated to average 1 hour per response, including the time for reviewing instructions, searching existing data sources, gathering and maintaining the data needed, and completing and reviewing the collection of information. Send comments regarding this burden estimate or any other aspect of this collection of information, including suggestions for reducing this burden, to Washington Headquarters Services, Directorate for Information Operations and Reports, 1215 Jefferson Davis Highway, Suite 1204, Arlington, VA 22202-4302, and to the Office of Management and Budget, Paperwork Reduction Project (0704-0188), Washington, DC 20503.

1. AGENCY USE ONLY (Leave blank)	2. REPORT DATE December 1994	3. REPORT TYPE AND DATES COVERED Final Technical Report 15 Aug 92 to 14 Dec 94

4. TITLE AND SUBTITLE Feedback Control of Vortex Flow	5. FUNDING NUMBERS F49620-92-J-0471

6. AUTHOR(S)
Peter A. Monkewitz

7. PERFORMING ORGANIZATION NAME(S) AND ADDRESS(ES) Department of Mechanical, Aerospace and Nuclear Engineering University of California, Los Angeles Los Angeles, CA 90095-1597	8. PERFORMING ORGANIZATION REPORT NUMBER

9. SPONSORING/MONITORING AGENCY NAME(S) AND ADDRESS(ES) AFOSR/NA 110 Duncan Avenue, Rm B115 Bolling AFB, DC 20332-8050	10. SPONSORING/MONITORING AGENCY REPORT NUMBER F49620-92-J-0471

11. SUPPLEMENTARY NOTES

12a. DISTRIBUTION AVAILABILITY STATEMENT Approved for public release; distribution unlimited.	12b. DISTRIBUTION CODE

13. ABSTRACT (Maximum 200 words)

The purpose of this overview is to show the utility of simple amplitude equations for the modelling of various vortex shedding phenomena. After a review of global modes which leads to the physical concept of local self-excited oscillators that act as "generators" of Karman vortices in the near wake, the characterization of the vortex street by a single Stuart-Landau oscillator is discussed. The success beyond expectation of this model as well as the problems associated with it are documented. Among them, we focus on the neglect of spatial structure in the simple temporal Stuart-Landau model. The role of spatial structure in the streamwise direction is highlighted by a short discussion of the effect of feedback control, while in the last part of the paper the model is extended to include the spanwise structure of vortex shedding, in particular the effect of the cylinder ends.

19971119 111   DC QUALITY INSPECTED 3

14. SUBJECT TERMS			15. NUMBER OF PAGES 49
			16. PRICE CODE

17. SECURITY CLASSIFICATION OF REPORT Unclassified	18. SECURITY CLASSIFICATION OF THIS PAGE Unclassified	19. SECURITY CLASSIFICATION OF ABSTRACT Unclassified	20. LIMITATION OF ABSTRACT UL

Standard Form 298 (Rev. 2-89) (EG)
Prescribed by ANSI Std. 239.18
Designed using Perform Pro, WHS/DIOR, Oct 94

FINAL TECHNICAL REPORT

For AFOSR Grant F 49620-92-J-0471

FEEDBACK CONTROL OF VORTEX FLOW

Performance Period: 08/15/92 - 12/14/94

P.I.: Peter A. Monkewitz

Dept. of Mechanical, Aerospace and Nuclear Engineering
UCLA, Box 951597
Los Angeles, CA 90095-1597

Current address:
Dept. of Mechanical Engineering
IMHEF-Ecublens
Swiss Federal Institute of Technology
CH-1015 Lausanne
SWITZERLAND
Fax: 01141 21 693 3281

I. GENERAL INTRODUCTION

During the period of thid grant, the general theory of globally unstable modes, i.e. temporally growing or self-excited modes with a two- or three-dimensional modal structure on a spatially evolving mean flow have been further developed. An account of the most recent developments is given in section II which is a reproduction of an invited lecture at the international colloquium on jets, wakes and shear layers held in April 1994 at CSIRO, Highett, Australia.

In this spirit, an investigation of the breakdown of a delta vortex has been undertaken. In a first step an experimental survey of vortex breakdown on a delta wing with 70° sweep has been carried out in the low-speed wind tunnel at UCLA. This survey, described in section III, has identified the conditions of breakdown as a function of angle of attack and the deflection of a trailing edge flap by flow visualization. Due to the departure of the P.I. from UCLA, this initial experimental investigation came to an end in mid 1993 and further experiments, in particular with active control, were rendered impossible during the report period.

On the theoretical side, work has begun on the analytical description of the instability that leads to vortex breakdown. As usual, the first step in such an analysis is the investigation of the linear stability of local profiles which is needed for the subsequent global mode analysis. During the report period, such local calculations have been carried out on mean flows typical for a breakdown structure. The first new result, reported in section IV, is the discovery of absolute instability in the breakdown region which bodes well for a future global mode analysis. As discussed in section IV, the stability analysis has been carried out on an assumed mean flow corresponding to breakdown. Therefore we cannot at this point explain why the breakdown structure forms in the first place, but we are hopeful that this might become possible as the investigation progresses.

II. MODELLING OF SELF-EXCITED WAKE OSCILLATIONS BY AMPLITUDE EQUATIONS

Peter A. Monkewitz
Dept. of Mechanical Engineering
Swiss Federal Institute of Technology, CH-1015 Lausanne, Switzerland

ABSTRACT

The purpose of this overview is to show the utility of simple amplitude equations for the modelling of various vortex shedding phenomena. After a review of global modes which leads to the physical concept of local self-excited oscillators that act as "generators" of Kármán vortices in the near wake, the characterization of the vortex street by a single Stuart-Landau oscillator is discussed. The success beyond expectation of this model as well as the problems associated with it are documented. Among them, we focus on the neglect of spatial structure in the simple temporal Stuart-Landau model. The role of spatial structure in the streamwise direction is highlighted by a short discussion of the effect of feedback control, while in the last part of the paper the model is extended to include the spanwise structure of vortex shedding, in particular the effect of the cylinder ends.

1. INTRODUCTION - A BRIEF REVIEW OF GLOBAL MODE CONCEPTS

Research on vortex shedding from bluff bodies has, over the last decade, received new impulses from the theory of hydrodynamic instability. The concept of local absolute and convective instability in particular, pioneered by Briggs [1] in the context of plasma instabilities, has proved useful in shear flows. The initial ideas about the possible connection between local absolute instability [2-4] and self-excited or time-amplified global oscillations of the entire near-wake have been refined in numerous publications (see for instance [5]). These theoretical ideas have gained importance due to the experimental discovery of Mathis et al. [6] and Provansal et al. [7] that Kármán vortex shedding is indeed a limit-cycle oscillation of the near-wake, resulting from a time-amplified global instability. They showed that the wake dynamics could be described by a single Stuart-Landau (S-L) equation [8] by measuring all coefficients of the S-L equation for a range of Reynolds numbers near the onset of Kármán shedding. Since then, experiments of this type have been repeated and refined by Sreenivasan et al. [9], Strykowski & Sreenivasan [10], Schumm [11] and Schumm et al. [5] for the wake and by Raghu & Monkewitz [12] for a heated jet.

When considering the stability properties of a two-dimensional basic flow which evolves in the streamwise direction, the so-called locally parallel approach is commonly used. For this, one takes the local mean velocity profile at a fixed streamwise location and considers the stability of a hypothetical parallel flow of infinite streamwise extent with a velocity profile equal to the selected local profile. Obviously the selection of streamwise location for the locally parallel analysis is arbitrary and hence the connection between the local analyses and

the "true" instability of the nonparallel flow remains unclear. In the context of linear stability this true instability is referred to as "global mode". It is simply a time-harmonic solution (allowing for temporal growth or decay) of the governing equations, linearized around a two-dimensional nonparallel basic wake flow, say $\underline{U}_0(x,y)$. The coordinate x is thereby pointing in the downstream direction and the two-dimensional biuff body producing the wake is aligned with the coordinate z. Hence, the total velocity field up to linear order in the perturbation is given by

$$\underline{U}(x,y,z,t) = \underline{U}_0(x,y) + \underline{\hat{u}}(x,y,z) \exp(-i\omega_G t) + O(|\underline{\hat{u}}|^2) \; , \tag{1}$$

where ω_G is the complex global frequency. Depending on the sign of the imaginary part of ω_G, the global mode is stable [$Im(\omega_G)<0$] or unstable [$Im(\omega_G)>0$]. Here and in the following (except in section 4 where an additional rescaling is introduced) all quantities are non-dimensional with D^*, the cylinder diameter or characteristic thickness of the bluff body, and the diffusion time D^{*2}/v^*, where the star indicates a dimensional quantity.

Under the assumption that a typical instability wave length λ is much shorter than the distance Λ over which the basic flow changes significantly, i.e that $\varepsilon\equiv\lambda/\Lambda \ll 1$ (in the context of bluff-body wakes, Λ may be defined on the basis of the centerline velocity U_c as $[d(U_c/U_\infty)/dx]^{-1}$), and that there is no long-range pressure feedback such as in edge-tone phenomena, a connection between local and global stability characteristics can be established by asymptotic WKBJ methods. This connection has been analysed by Huerre & Monkewitz [13], Chomaz, Huerre & Redekopp [14], Hunt & Crighton [15], Soward [16], Monkewitz, Huerre & Chomaz [17] and LeDizès et al. [18, 19] who have shown that local absolute instability over some streamwise interval of the nonparallel flow is necessary for global instability. The details of the linear analysis are rather involved but stand on a sound mathematical basis. The weakly nonlinear extension of the global mode analysis, on the other hand, has so far only been possible under very restrictive assumptions [18, 20] and is still under investigation. The essence of the results can be summarized (see also Albarède & Monkewitz [21]) in the following (over)simplified form: allowing for weak spanwise variations, any suitably scaled disturbance quantity Δ can be represented as

$$\Delta = A(T,Z) \, B(\xi) \, C(y;x^t) \exp[i\omega_G t - ik^t(x - x^t)] + c.c. \; , \tag{2}$$

where c.c. stands for the complex conjugate and x^t is a turning point (point of breakdown) of the WKBJ formulation, assuming here that there is only one which acts as a "generator of waves" with wave number k^t for the entire flow. This wave-maker region extends over a flow interval $|\xi|\leq O(1)$, where $\xi = \varepsilon^\alpha(x-x^t)$ with $\alpha=1/2$ for flows dominated by a maximum of the absolute growth rate within the flow domain and $\alpha=1/3$ for flows dominated by absolute instability at a streamwise flow boundary [17]. The function C in (2) represents the cross-stream structure of the disturbance which is frozen at x^t and is nothing but the eigenfunction of the conventional local parallel stability problem. B represents the linear global mode shape or the envelope of the carrier wave $\exp[i\omega_G t - ik^t(x - x^t)]$ which is assumed to be independent of the spanwise location z. As shown by Huerre & Monkewitz [13] and Monkewitz et al. [17], the envelope B of the most unstable global mode is established on a time scale $\tau=\varepsilon^{2\alpha} t$, starting from an infinitesimal initial disturbance. The overall amplitude A finally describes the weakly nonlinear evolution of the global mode on the time scale $T=\varepsilon^{2\beta} t$, which is slower

than τ ($\beta>\alpha$), as well as the weak coupling between "oscillators" at different spanwise locations which leads to slow amplitude variations on the scale $Z=\epsilon^\beta z$.

Since we can restrict ourselves, as shown by Mathis et al. [6] and Provansal et al. [7], to the case of a super-critical Hopf bifurcation (see e.g. [8]), i.e. to the case when a linearly unstable global mode evolves continuously into limit-cycle oscillations, the saturation time scale can always be made slower than the time for the establishment of the linear global mode shape. It is therefore meaningful to consider the evolution of an initial impulse in a nonparallel flow as a "two-step" process: the first step consists of the impulse evolving into the most unstable linear global mode by the process of selective amplification, assuming that the "critical" mode grows much faster than all the "higher" global modes. The second step involves a period during which the critical linear global mode grows exponentially *as a whole* at the rate $Im(\omega_G)$, followed by nonlinear saturation and diffusion in the Z-direction which is *fully described by the overall amplitude* A(T,Z) governed by the Ginzburg-Landau (G-L) equation.

$$\partial_T A = [\sigma_r + i\sigma_i]A + [\mu_r + i\mu_i]\partial_{ZZ}A - [l_r + il_i]|A|^2A \quad . \tag{3}$$

This equation reduces to the S-L equation when A is independent of Z which is the topic of the next section. The governing equation for the linear mode shape B and its implications will be discussed in section 3 and the mechanism leading to spanwise variations of A is tackled in section 4. At this point again, it has to be made absolutely clear that *equation (3)* in particular *can so far only be derived in a rational manner under extremely restrictive conditions and can therefore only be considered as a MODEL EQUATION for the practical applications* to follow!

2. THE UNEXPECTED SUCCESS OF THE STUART-LANDAU MODEL FOR THE DESCRIPTION OF VORTEX SHEDDING TRANSIENTS

For strictly two-dimensional vortex shedding, equation (3) reduces to the well known S-L equation which is written below in terms of the modulus $|A|$(T) and phase Φ(T) of the complex amplitude $A=|A| \exp(i\Phi)$:

$$|A|^{-1}d_T|A| = \sigma_r - l_r|A|^2 = \sigma_r[1 - (|A| / |A|_{sat})^2] \quad , \tag{4a}$$

$$d_T\Phi = \sigma_i - l_i|A|^2 = \sigma_i - (\sigma_r l_i / l_r)(|A| / |A|_{sat})^2 \quad , \tag{4b}$$

$$|A|_{sat} = [\sigma_r/l_r]^{1/2} = \{[d\sigma_r/dR](R_{cr}) / l_r\}^{1/2} [R-R_{cr}]^{1/2} \quad . \tag{4c}$$

This form of the equation, with $|A|^{-1}d_T|A|$ and $d_T\Phi$ representing the instantaneous growth rate and frequency respectively, pertains to a supercritical Hopf bifurcation, i.e. to a situation with $l_r>0$ where the nonlinearity is amplitude-limiting. Furthermore it is clear that the introduction of the saturation or limit-cycle amplitude $|A|_{sat}$ is only permissible in an unstable situation $\sigma_r>0$. It is repeated here that these equations are only meaningful if they describe the evolution of a global mode as a whole, i.e. if the linear growth rate σ_r, the linear frequency σ_i and the nonlinear frequency correction ($\sigma_r l_i / l_r$) are *independent of the measuring location*. l_r on the other hand does depend on the choice of measuring location which amounts to a particular normalization of the streamwise global mode shape B.

Throughout the paper the coefficients of (4) will be assumed to depend exclusively on the Reynolds number $R=U^*_\infty D^*/v^*$, which plays the role of bifurcation parameter. As discussed by Stuart [8], the balance of terms in (4a) requires that the linear growth rate σ_r be small of order $O(|A|^2)$. Hence the "distance from criticality" $(R-R_{cr})$ has to be of order $O(|A|^2)$, where R_{cr} is defined by $\sigma_r(R_{cr})=0$, and it is consistent to approximate the coefficients in (4) by

$$\sigma_r = [R-R_{cr}][d\sigma_r/dR](R_{cr}) + O(|R-R_{cr}|^2) \ ,$$

$$\sigma_i = \sigma_i(R_{cr}) + [R-R_{cr}][d\sigma_i/dR](R_{cr}) + O(|R-R_{cr}|^2) \ , \qquad (5)$$

$$[l_r+il_i] = [l_r+il_i](R_{cr}) + O(|R-R_{cr}|) \ .$$

To illustrate the success of this model in the wake, we discuss the case of a circular cylinder (L/D=50) with base bleed, shown on fig.1a. To rapidly shut off or start the base bleed, the supply lines on both ends were fitted with solenoid valves. Figure 1b shows the critical Reynolds number as a function of base bleed coefficient, defined by $c_b=Q^*/(L^* D^* U^*_\infty)$ with Q the discharge through the slot. At high R, the critical bleed coefficient asymptotes at $c_b=0.12$ which is consistent with Monkewitz and Nguyen's [22] result that typical inviscid wake profiles become convectively unstable at a bleed coefficient of 9% . At the low-R end, the wake can be destabilized down to R=27 which is consistent with the observations of Berger [23] and Nishioka & Sato [24], that no stable vortex streets can be excited below Reynolds numbers of around 20 to 25. We must conclude that around R=27 the suction has to be so strong that the global mode damping due to nonparallel effects overcomes the destabilizing effect of increased reverse flow. The sudden interruption of base bleed or base suction are now used to produce transients. This is first shown on the smoke wire visualizations of figure 2, where the first frame shows the initial total suppression of vortex shedding with a bleed coefficient of 0.10 at Re=68.

The coefficients of the SL-equation are deduced by fitting the relations 4a and 4b to the instantaneous growth rate and frequency that are obtained by a complex demodulation of the measured velocity trace during transients as described for instance by Raghu & Monkewitz [12] and Schumm et al. [5]. A typical transient is shown on fig. 3 and the resulting linear growth rate, frequency and Landau constant are displayed on fig. 4. Numerically we find

$$R_{cr} = 46.7 \pm 0.3 \ , \qquad (6a)$$

$$\sigma_r = [0.21 \pm 0.005] (R-R_{cr}) \ , \qquad (6b)$$

$$\sigma_i = [33.6 \pm 0.3] + [0.64 \pm 0.02] (R-R_{cr}) \ , \qquad (6c)$$

$$l_i/l_r = -[2.90 \pm 0.45] \ . \qquad (6d)$$

First we note that the slope of the growth rate (6b) is somewhat higher than the value of 0.20 published by Provansal et al. [7] and Strykowski & Sreenivasan [10]. This slight increase appears due to the fact that we have consistently extrapolated growth rates to zero amplitudes. We also note the excellent agreement between the data obtained with base bleed and with shedding suppression by cylinder oscillations [5]. The Landau constant (6d) also is consistent with the value of -3, published by Sreenivasan et al. [9].

With equ. (4b), the results (6a) to (6d) can also be combined to yield the saturation frequency. After division by $(2\pi R)$ we obtain the Roshko relation for the Strouhal number S

$$S \equiv f^* D^* / U^*_\infty = -3.94/R + 0.199 \ . \tag{7}$$

The numerical coefficients can be compared to the values given by Williamson [25] after his equation (6). We find that our values are closer to his three-term than his two-term fit. Near the bifurcation, where the S-L equation is valid, (7) is indistinguishable from Williamson's fits, while it falls only slightly below his universal curve at R=100. This supports our observation that the transients are not contaminated by three-dimensional effects.

The first comment pertains to the range of R over which the measured coefficients follow the leading order relation (5). As already said, the S-L equation can only be justified very close to R_{cr} and it is an open question why it still applies at $1.3R_{cr}$ and beyond. This is even more surprising in view of the discussion of "higher" global modes in section 3 and may be an accident altogether.

Next, the question must be asked whether it is legitimate to characterize the global mode amplitude by a single measurement at a fixed location. This has been addressed by Goujon-Durand et al. [26] who started from the idea that the most obvious way of characterizing the global mode should be by its maximum amplitude with respect to x. To their surprise they found that the maximum saturation amplitude $|A|_{sat}|B|_{max}$ scaled like $(R-R_{cr})$ to the *first* and not the one-half power as suggested by (4c). Investigating further, they found that the location x_{max} where $|B|$ has its maximum scaled like $(R-R_{cr})^{-1/2}$ such that only $|A|_{sat}\int |B|dx$ scales like the expected $(R-R_{cr})^{1/2}$ over the range $R=R_{cr}$ to $1.84\ R_{cr}$. However, this finding does not jeopardize the measurements of the linear growth rates, linear frequencies and nonlinear frequency correction which have been found independent of measuring location by Schumm [11] (see also [5, 27]). Furthermore, the scaling of the amplitude with $(R-R_{cr})^{1/2}$ found by Mathis et al. [6], Provansal et al. [7] and Schumm et al. [5] may be explained by the fact that in all cases the measurement location was situated in the "tail" of the global mode, typically at 10D, where the scaling of $|A|_{sat}|B|(x=10D)$ is quite close to $(R-R_{cr})^{1/2}$ (see also fig. 4 of Ohle & Eckelmann [28]).

Finally one may ask whether it is not possible to compute at least the coefficients (6a) and (6b) from local linear stability properties of the wake following to the formalism of Monkewitz et al. [17]. This has been attempted by S. LeDizès and this author with the following result: the local absolute growth rate, shown on fig. 6, associated with velocity profiles computed by Morzynski & Thiele [29] shows a weak maximum within the flow domain but virtually no reduction towards the base of the cylinder. Therefore, the cylinder wake does not fall into the category of flows dominated by a maximum of absolute growth rate at a boundary nor the one dominated by a maximum within the flow. Such a situation is not amenable to the semi-analytic treatment of Monkewitz et al. [17] and it does not seem possible to progress beyond qualitative statements, as given in Monkewitz [30] for instance.

3. THE MODELLING OF FEEDBACK CONTROL

In this section the effect of proportional feedback control is used to illustrate the existence of multiple global modes. The control is effected by taking the signal from a single downstream sensor and feeding it, after appropriate amplification g and phase shift γ, to an actuator which can be the cylinder itself that is oscillated, a speaker or some other device [27]. As Berger [23, 31] has shown, the Kármán street can be suppressed over a limited Reynolds number range by feedback. To understand the behaviour of such self-excited systems with feedback, Monkewitz [32] (see also Lee [33] and the similar study by Park et al. [34]) has used the governing equation for the linear global mode shape B in a doubly-infinite domain (Huerre & Monkewitz [13])

$$\partial_\tau B + P_0\, \partial_{\xi\xi}B + P_1(\xi)\, \partial_\xi B + P_2(\xi)\, B = g\, \exp(i\gamma)\, \delta(\xi-\xi_a)\, B(\xi=\xi_s)\ ,\quad B(|\xi| \to \infty) = 0\ ,\quad (8)$$

where the P_n are polynomials of degree n, ξ_a is the actuator location and ξ_s is the sensor location. When looking for time-harmonic solutions, this represents an eigenvalue problem in x which admits an infinity of eigenmodes (with the frequency as eigenvalue). The finding of the study, later experimentally confirmed in detail by Monkewitz et al. [35] (see also [27]) and Roussopoulos [36, 37], is that suppression of self-excited vortex shedding is only possible close to R_{cr} because the conflicting requirements on gain and phase to suppress the unstable Kármán mode and *not to excite* any "higher" global modes cannot be resolved beyond some R which is typically not more than 10% above R_{cr}. This serves to show that in the wake, as well as in many other self-excited fluid systems, there are global modes with only slightly smaller growth rates and quite similar mode shapes "waiting in the wings" to be destabilized. This makes one wonder again why the S-L model, which describes the evolution of a *single* mode, is so successful. It may be that all the higher modes are suppressed by some nonlinear mechanism once the most unstable mode reaches finite amplitude. It is however also conceivable, that the measurements described in the last section are of a "composite" nature, smoothing over mode switches that are screened by experimental noise and the incomplete survey of the flow field.

4. VORTEX SHEDDING FROM FINITE-LENGTH CYLINDERS - PHASE DYNAMICS

Finally, we return to the full G-L equation (3) for the overall amplitude A which includes the diffusive coupling of "oscillators" along the span. This equation has already been discussed extensively by Albarède & Monkewitz [21] and similar models have been considered by Noack et al. [38]. In physical terms, the use of the spanwise G-L equation amounts to representing the streamwise formation region of Kármán vortices as a line source. The time evolution of the source strength is then directly associated with the observed spatial pattern by a "Taylor hypothesis", i.e. by replacing t with $(-x/U_c)$, where $U_c \approx 0.88\, U_\infty$ is the virtually constant streamwise convection speed of the Kármán vortices (Fig. 9b of Williamson [25]). Hence the visualization of the vortex pattern in the x-z plane provides the ideal "strip-chart recording" of the source dynamics and each vortex marked by the tracer (smoke) delineates a line of constant phase in the $(-x/U_c)$-z plane.

The main result of Albarède & Monkewitz [21] is the elucidation of the role of end conditions in determining the angle of oblique shedding. In particular, they have shown that parallel shedding is induced by an increase of the degree of instability towards the ends, which corresponds in practical terms to an increase of Reynolds number and/or to a decrease of the base pressure (see Williamson & Roshko [39]). In the following we will concentrate on the phase dynamics of the Kármán vortices away from the ends, assuming that the shedding angle or spanwise wave number imposed by the actual end condition is known. For this, it is useful to recast equation (3) in terms of modulus and phase, undoing at the same time the scalings of t and z with ε and introducing a convenient nondimensionalization:

$$\partial_t M = M + \partial_{zz}M - M(\partial_z\Phi)^2 - c_1 M^{-1}\partial_z(M^2\partial_z\Phi) - M^3 \quad , \tag{9a}$$

$$M\partial_t\Phi - c_2\partial_t M = c_\Delta [\partial_{zz}M - M(\partial_z\Phi)^2] + c_\varphi M^{-1}\partial_z(M^2\partial_z\Phi) \quad , \tag{9b}$$

with $A / A_{ref} = M(t,z) \exp[i\Phi(t,z) + i(c_0 - c_2)t]$,

$$c_0 = \sigma_i/\sigma_r \ , \quad c_1 = \mu_i/\mu_r \ , \quad c_2 = l_i/l_r \ , \quad c_\varphi = 1 + c_1c_2 \ , \quad c_\Delta = c_1 - c_2$$

Assuming that the original A has already been made nondimensional with a suitable reference of the measured physical quantity, the reference quantities for the above nondimensionalization are $A_{ref} = (\sigma_r / l_r)^{1/2}$, $t_{ref} = \sigma_r^{-1}$, $z_{ref} = (\mu_r / \sigma_r)^{1/2}$.
The amplitude is thus scaled with the two-dimensional saturation amplitude (see equ. 4c), the time with the e-fold growth time of the 2-D instability and z with the spanwise diffusion length.

Since in this paper we are only interested in the region away from the ends where M is close to unity, equation (9) can be further simplified. Expanding (9) for small spanwise wave numbers $q=\partial_z\Phi$ and taking into account that $\partial_z=O(q_{ref})$ and $\partial_t=O(q^2_{ref})$ one finds

$$\partial_t\Phi = -c_\Delta(\partial_z\Phi)^2 + c_\varphi \partial_{zz}\Phi + W \partial_z\Phi + O(q^4_{ref}) \quad , \tag{10a}$$

$$M = 1 - (1/2)[(\partial_z\Phi)^2 + c_1\partial_{zz}\Phi] + O(q^4_{ref}) \quad . \tag{10b}$$

From this point on we will only deal with the simplified equation (10a) which is equivalent to Burgers equation and in which a convective term has been added to represent a small (at most of order q_{ref}) spanwise flow W imposed by the end conditions.

Oblique shedding and phase shocks

The simplest solution of (10a) is the plane wave solution

$$q = \partial_z\Phi = const. \text{ with the frequency correction } \partial_t\Phi = -c_\Delta q^2 + W q \ , \tag{11}$$

where the spanwise wave number is related to the shedding angle Θ by $q = 2\pi\sin(\Theta) / \lambda_0$ with λ_0 the streamwise wave length that can be taken from fig. 9a of [25]. Spanwise regions of different shedding angle can now be connected through a phase shock that corresponds to

the well known shock solution of Burgers equation. Assigning the indices "1" and "2" to the regions behind and in front of the shock, respectively, it is given by

$$q(t,z) = (q_1+q_2)/2 - [(q_1-q_2)/2] \tanh[\delta^{-1}(z-U_s t)] \quad , \tag{12}$$

$$\delta = 2c_\varphi \, [c_\Delta(q_1-q_2)]^{-1} \quad , \quad U_s = c_\Delta(q_1+q_2) \quad , \quad W = 0 \quad . $$

For a shock solution to exist, the shock thickness δ has to be positive, i.e. $(q_1-q_2)>0$. In other words, the region with larger shedding angle always "eats" into the region with the smaller angle. To start a shock, one of the end conditions needs to be changed in a step fashion. This is easily achieved with the suction tube technique of Miller & Williamson [40] where the amount of suction can be varied within a few Kármán cycles. Figure 7 shows such a shock, initiated (before the photo was taken) by a sudden decrease of the suction at the upper edge of the figure. On this "strip-chart recording" the time origin is roughly 110 Kármán wave lengths beyond the right hand edge of the frame and in the final state the oblique shedding with the larger angle extends over the entire span. The velocity U_s of phase shocks has been measured for various initial and final angles (Monkewitz, Williamson & Miller [41]). With model constants deduced from the frequency correction (11) for oblique shedding, which is indistinguishable from Williamson's $\cos(\Theta)$ law [25] over all observed angles (the maximum angle being around 25°), the prediction (12) is in good agreement with the measurements (see [41]) and yields in physical variables $U_s/U_\infty = 0.44 \{\sin(\Theta_1) + \sin(\Theta_2)\}$, with Θ_1 and Θ_2 the shedding angles behind and in front of the phase shock.

The "reverse bow" of Kármán vortices

A second phenomenon that can be easily explained by the model (10a) is the small reverse bow often found when end conditions are adjusted for parallel shedding and first documented by Hammache and Gharib [42]. Their flow visualization is reproduced here as fig. 8. The model forbids any propagation of regions of reverse angle away from the ends and suggests the following most likely cause: since parallel shedding is induced by *lowering* the base pressure towards the ends, a spanwise mean flow towards both ends must be generated that can become significant especially if the lowering of the pressure is "overdone". Assuming for W the functional form (13a), one finds the exact solution (13b) of (10a) which represents a parabolic reverse bow of the lines of constant phase.

$$W(z) = w \, (2z/L - 1) \quad , \tag{13a}$$

$$q(z) = (w/c_\Delta) \, (2z/L - 1) \quad , \quad \partial_t \Phi = 2w/(c_\Delta L) \quad . \tag{13b}$$

For an extreme case, that unfortunately does not correspond to any of their flow visualization, Hammache and Gharib [42, their fig. 13] have measured this velocity at $z=0.26L$ and $z=0.74L$ to be around 3% of U_∞ at the y-location of the Kármán vortices. This, together with the model coefficients determined from the frequency law (11) and the phase shock experiments yields a reverse shedding angle of around 16° at both cylinder ends which is consistent with the observation (private communication of M. Hammache). The frequency correction (13b) associated with the reverse bow on large aspect ratio cylinders (of the order of 100) is not measurable as it is of the order of 10^{-4} in terms of Strouhal number.

Phase expansions

For $(q_1-q_2)<0$ equation (10a) does not admit shock solutions. The question is therefore how an oblique shedding pattern can relax back to parallel shedding if the end conditions are readjusted. In analogy to gas dynamics (Burgers equation) the answer is clearly via a phase expansion fan. An experiment has been conceived [41] where initially one end condition at, say z=L is set for parallel shedding, while the second is set for some oblique shedding angle. As a consequence, the oblique shedding, having spread by a phase shock, initially occupies the entire span. At t=0 the second end condition at z=0 is also set for parallel shedding in an abrupt manner. As predicted by the model, this starts a phase expansion fan moving across the span and ultimately leads to parallel shedding everywhere. This process is illustrated by the flow visualization of fig. 9.

A preliminary quantitative test of the model has been performed on such phase expansions. The coefficients of the model have thereby been chosen solely on the basis of experiments with oblique shedding and phase shocks. At R=120 the resulting coefficients are in dimensional form $c_\Delta \mu^*_r /v^* = 44$, $\mu^*_r /(\sigma^*_r D^{*2}) = 1.1$ and $c_\varphi /c_\Delta \approx 1$. Equation (10a) with W=0 has been integrated with these coefficients and half a "chevron" (see [21]) between z=0 and L as initial condition. Fortunately it turns out that the results are quite insensitive to the value of c_φ /c_Δ which could not be determined accurately. The preliminary results are shown on fig. 10 in terms of the time history of the spanwise wave number q(t) at the fixed spanwise position z=L/4, normalized by the initial spanwise wave number q_0. This comparison reveals that the early portion of the phase expansions is very well predicted by the model, while the computed tails consistently fall off too slowly. The reasons for this sytematic deviation is still under investigation.

5. CONCLUSIONS

It has been shown, that the amplitude equations presented in this paper allow at least a qualitative understanding of many aspects of the wake dynamics, in particular of the evolution of shedding patterns. If properly calibrated by experiments, i.e. with experimentally determined coefficients, the models even provide a consistent quantitative description of many shedding phenomena that could otherwise only be obtained numerically at considerable expense. Therefore we believe that this approach provides a valuable tool for investigating the parametric dependence of known shedding phenomena as well as for conceiving new experiments. One such experiment stimulated by the study of the G-L equation (3) with *periodic* boundary conditions has been the investigation of the ring wake by Leweke et al. [43]. An area where considerable progress seems possible through the analysis of amplitude equations is the shedding from cylinders with slowly varying diameter, such as slender cones. So far, the model defined by equation (3) with a suitably varying $\sigma(z)$ has been integrated numerically by Noack et al. [38] and Papangelou [44] to show qualitatively the formation of cells of different shedding frequency along the span. However, very little is known yet about the scaling properties of such cells. Another promising area with a potentially wide range of application is the elucidation of three-dimensional effects induced by local feedback [36, 37].

ACKNOWLEDGEMENTS

NOMENCLATURE

All quantities are non-dimensional with D^* and the diffusion time D^{*2}/ν^*

A, B, C	complex amplitude functions
c_b	base bleed coefficient
D^* [m]	cylinder diameter
f^* [sec^{-1}]	frequency
k	streamwise wave number
L	cylinder length
L^* [m]	dimensional cylinder length
l	complex coeff. of nonlinear term in the G-L equ.
Q^* [m^3/sec]	volume flow rate of base bleed
q	spanwise wave number
R	Reynolds number
S	Strouhal number
t, T, τ	time (with different scalings)
$\underline{U}, \underline{u}$	velocity vector
U_c	centerline velocity
U_∞	freestream velocity
U^*_∞ [m/sec]	dimensional freestream velocity
W	mean spanwise velocity
x, ξ	streamwise coordinate (with different scalings)
y	cross-stream coordinate
z, Z	spanwise coordinate (with different scalings)
Δ	arbitrary disturbance quantity
$\varepsilon \equiv \lambda/\Lambda$	small nonparallelism parameter
Φ [rad]	phase of complex amplitude function A
Λ	mean flow evolution length
λ	typical instability wave length
$\mu = \mu_r + i\,\mu_i$	complex coeff. of diffusion in the G-L equ.
μ^*_r [m^2/sec]	dimensional real part of the coeff. of diffusion in the G-L equ.
ν^* [m^2/sec]	kinematic viscosity
Θ [rad]	vortex shedding angle
$\sigma = \sigma_r + i\,\sigma_i$	complex growth rate in the G-L equ.
σ^*_r [sec^{-1}]	dimensional real part of the growth rate in the G-L equ.
ω	radian frequency
ω_G	global mode frequency

REFERENCES

1. Briggs, R.J., *Electron-stream interaction with plasmas*, MIT Press, 1964.

2. Pierrehumbert, R.T., Local and global baroclinic instability of zonally varying flows. J. Atmos. Sci. **41**, 2141-2162, 1984.

3. Koch, W., Local instability characteristics and frequency determination of self-excited wake flows. J. Sound Vib. **99**, 53-83, 1985.

4. Huerre, P. & Monkewitz, P.A., Absolute and convective instabilities in free shear layers. J. Fluid Mech. **159**, 151-168, 1985.

5. Schumm, M., Berger, E. & Monkewitz, P.A., Self-excited oscillations in the wake of two-dimensional bluff bodies and their control. J. Fluid Mech. **271**, 17-53, 1994.

6. Mathis, C., Provansal, M. & Boyer, L., The Bénard-von Kármán instability: an experimental study near the threshold. J. Physique Lett. (Paris) **45**, L483-L491, 1984.

7. Provansal, M., Mathis, C. & Boyer, L., Bénard-von Kármán instability: transient and forced regimes. J. Fluid Mech. **182**, 1-22, 1987.

8. Stuart, J.T., Nonlinear stability theory. Ann. Rev. Fluid Mech. **3**, 347-370, 1971.

9. Sreenivasan, K.R., Strykowski, P.J. & Olinger, D.J., Hopf bifurcation, Landau equation and vortex shedding behind circular cylinders. In *Proc. Forum on Unsteady Flow Separation* (Ed. K.N. Ghia), 1-13, ASME, 1986.

10. Strykowski, P.J. & Sreenivasan, K.R., On the formation and suppression of vortex shedding at low Reynolds number. J. Fluid Mech. **218**, 71-107, 1990.

11. Schumm, M., Experimentelle Untersuchungen zum Problem der absoluten und konvektiven Instabilität im Nachlauf zweidimensionaler stumpfer Körper. Ph.D. thesis no. D83 - FB 09, Technical University Berlin. Published in VDI - Fortschrittsberichte Reihe 7, no. 196, VDI - Verlag Duesseldorf, 1991.

12. Raghu, S. & Monkewitz, P.A., The bifurcation of a hot round jet to limit-cycle oscillations. Phys. Fluids **A 3**, 501-503, 1991.

13. Huerre, P. & Monkewitz, P.A., Local and global instabilities in spatially developing flows. Ann. Rev. Fluid Mech. **22**, 473-537, 1990.

14. Chomaz, J.M., Huerre, P. & Redekopp, L.G., A frequency selection criterion in spatially developing flows. Studies Appl. Math. **84**, 119-144, 1991.

15. Hunt, R.E. & Crighton, D.G., Instability of flows in spatially developing media. Proc. R. Soc. Lond. **A 435**, 109-128, 1991.

16. Soward, A.M., Thin disc kinematic $\alpha\omega$-dynamo models II. Short length scale modes. Geophys. Astrophys. Fluid Dyn. **64**, 201-225, 1992.

17. Monkewitz, P.A., Huerre, P. & Chomaz, J.M., Global linear stability analysis of weakly nonparallel shear flows. J. Fluid Mech **251**, 1-20, 1993.

18. LeDizes, S., Modes globaux dans les écoulements faiblement inhomogènes. Ph.D. thesis, Ecole Polytechnique, Paris, 1994.

19. LeDizes, S., Huerre, P., Chomaz, J.M. & Monkewitz, P.A., Linear global modes in spatially-developing media. To appear in Phil. Trans. Royal Soc. London, 1994.

20. LeDizes, S., Monkewitz, P.A. & Huerre, P., Weakly nonlinear analysis of spatially developing shear flows. In *Bluff-Body Wakes, Dynamics and Instabilities* (H. Eckelmann, J.M.R. Graham, P. Huerre, P.A. Monkewitz, Eds.), pp. 148-152, Springer, Berlin, 1993.

21. Albarede, P. & Monkewitz, P.A., A model for the formation of oblique shedding and "chevron" patterns in cylinder wakes. Phys. Fluids **A 4**, 744-756, 1992.

22. Monkewitz, P.A. & Nguyen, L.N., Absolute instability in the near wake of two-dimensional bluff bodies. J. Fluids Struct. **1**, 165-184, 1987.

23. Berger, E. , Unterdrückung der laminaren Wirbelströmung und des Turbulenzeinsatzes der Kármán'schen Wirbelstrasse im Nachlauf eines schwingenden Zylinders. Jahrbuch der WGLR (H. Blenk, Ed.), pp. 164-172, Friedr. Vieweg, Braunschweig, 1964.

24. Nishioka, M. & Sato, H. , Mechanism of determination of the shedding frequency of vortices behind a cylinder at low Reynolds number. J. Fluid Mech. **89**, 49-60, 1978.

25. Williamson, C.H.K. , Oblique and parallel modes of vortex shedding in the wake of a circular cylinder at low Reynolds numbers. J. Fluid Mech. **206**, 579-627, 1989.

26. Goujon-Durand, S., Jenffer, P. & Wesfreid, J.E. , Downstream evolution of the Bénard - Von Kármán instability. Phys. Rev. E **50**, 308-313, 1994.

27. Monkewitz, P.A. , Wake control. In *Bluff-Body Wakes, Dynamics and Instabilities* (H. Eckelmann, J.M.R. Graham, P. Huerre, P.A. Monkewitz, Eds.), pp. 227-240, Springer, Berlin, 1993.

28. Ohle, F. & Eckelmann, H. , Modelling of a Kármán vortex street at low Reynolds numbers. Phys. Fluids **A 4**, 1707-1714, 1992.

29. Morzynski, M. & Thiele, F. , Numerical investigation of wake instabilities. In *Bluff-Body Wakes, Dynamics and Instabilities* (H. Eckelmann, J.M.R. Graham, P. Huerre, P.A. Monkewitz, Eds.), pp. 135-142, Springer, Berlin, 1993.

30. Monkewitz, P.A. , The absolute and convective nature of instability in two-dimensional wakes at low Reynolds numbers. Phys. Fluids **31**, 999-1006, 1988.

31. Berger, E. , Suppression of vortex shedding and turbulence behind oscillating cylinders. Phys. Fluids **10**, S191-S193 (Suppl.), 1967.

32. Monkewitz, P.A. , Feedback control of global oscillations in fluid systems. AIAA paper no. 89-0991, 1989.

33. Lee, C.K. , Feedback control of global oscillations in a bluff body wake. M.S. thesis, Univ. California, Los Angeles, 1992.

34. Park, D.S., Ladd, D.M. & Hendricks, E.W. , Feedback control of a global mode in spatially developing flows. Submitted to Phys. Lett. A, 1993.

35. Monkewitz, P.A., Berger, E. & Schumm, M. , The nonlinear stability of spatially inhomogeneous shear flows, including the effect of feedback. Eur. J. Mech. B/Fluids **10**, no.2 - Suppl., 295-300, 1991.

36. Roussopoulos, K. , Feedback control of vortex shedding at low Reynolds numbers. J. Fluid Mech. **248**, 267-296, 1993.

37. Roussopoulos, K. , Aspects of bluff body wake control. In *Bluff-Body Wakes, Dynamics and Instabilities* (H. Eckelmann, J.M.R. Graham, P. Huerre, P.A. Monkewitz, Eds.), pp. 249-252, Springer, Berlin, 1993.

38. Noack, B.R., Ohle, F. & Eckelmann, H. , On cell formation of vortex streets. J. Fluid Mech. **227**, 293-308, 1991.

39. Williamson, C.H.K. & Roshko A. , Measurement of the base pressure in the wake of a cylinder at low Reynolds number. Z. Flugwiss. Weltraumforschung **14**, 38-46, 1990.

40. Miller, G.D. & Williamson, C.H.K. , Control of three-dimensional phase dynamics in a cylinder wake. Submitted to Exp. in Fluids, 1994.

41. Monkewitz, P.A., Williamson, C.H.K. & Miller, G.D. , Phase dynamics of Kármán vortices in cylinder wakes. In preparation for Phys. Rev. Lett, 1994.

42. Hammache, M. & Gharib, M. , An experimental study of the parallel and oblique vortex shedding from circular cylinders. J. Fluid Mech. **232**, 567, 1991.

43. Leweke, T., Provansal, M. & Boyer, L. , Stability of vortex shedding modes in the wake of a ring at low Reynolds numbers. Phys. Rev. Lett. **71**, 3469-3472, 1993.

44. Papangelou, A. , Vortex shedding from slender cones at low Reynolds numbers. J. Fluid Mech. **242**, 299-321, 1992.

FIGURE CAPTIONS

Figure 1. a) Cross section of the cylinder with base bleed of dimension D=4mm and h=2mm. b) Critical bleed coefficient versus R with the two asymptotes indicated by broken lines (from Schumm et al. [5]).

Figure 2. Smoke visualization of wake transient (R=68) after switching off the base bleed. Frames are 200ms apart and the intersection of the light sheet with the cylinder is defined by its shadow (from Schumm et al. [5]).

Figure 3. Time history of streamwise velocity at (x/D,y/D)=(14,1) during a transient at R=48.5 . Distance between tick marks is 114 ms (from Schumm [11]).

Figure 4. Coefficients of S-L equation versus R for the circular cylinder. Δ, transients induced by interruption of base bleed; O, control of shedding by cylinder oscillations (from Schumm et al. [5]).

Figure 5. a) Maximum saturation amplitude and its location versus R: $\blacksquare$, $|A|_{sat}|B|_{max}$ (arb. units); O, x_{max}/D b) Collapse of global mode shapes at various R (from Goujon-Durand et al. [26], with permission).

Figure 6. Local absolute growth rate versus x/D for a cylinder wake at R=50.

Figure 7. Smoke visualization of phase shock for R=120 , L /D=200 (from [40, 41]). Flow is from left to right.

Figure 8. Reverse bow at R=100 (from Hammache & Gharib [42], with permission). Flow from top to bottom.

Figure 9. Smoke visualisation of phase expansion at R=120 (from [40, 41]). Flow is from left to right. The end condition at the lower edge is permanently set for parallel shedding while the one at the upper egde has been changed to parallel shedding at t=0 corresponding to a point about 10 Kármán wave lenths beyond the right hand edge of the frame.

Figure 10. Time history of normalized spanwise wave number at z=L/4 during a phase expansion initiated at t=0, with initial shedding angles of 10° and 20° and R=120 (D=1.08mm , L/D=200). The model computations are shown as broken lines.

(a) U_∞ h D
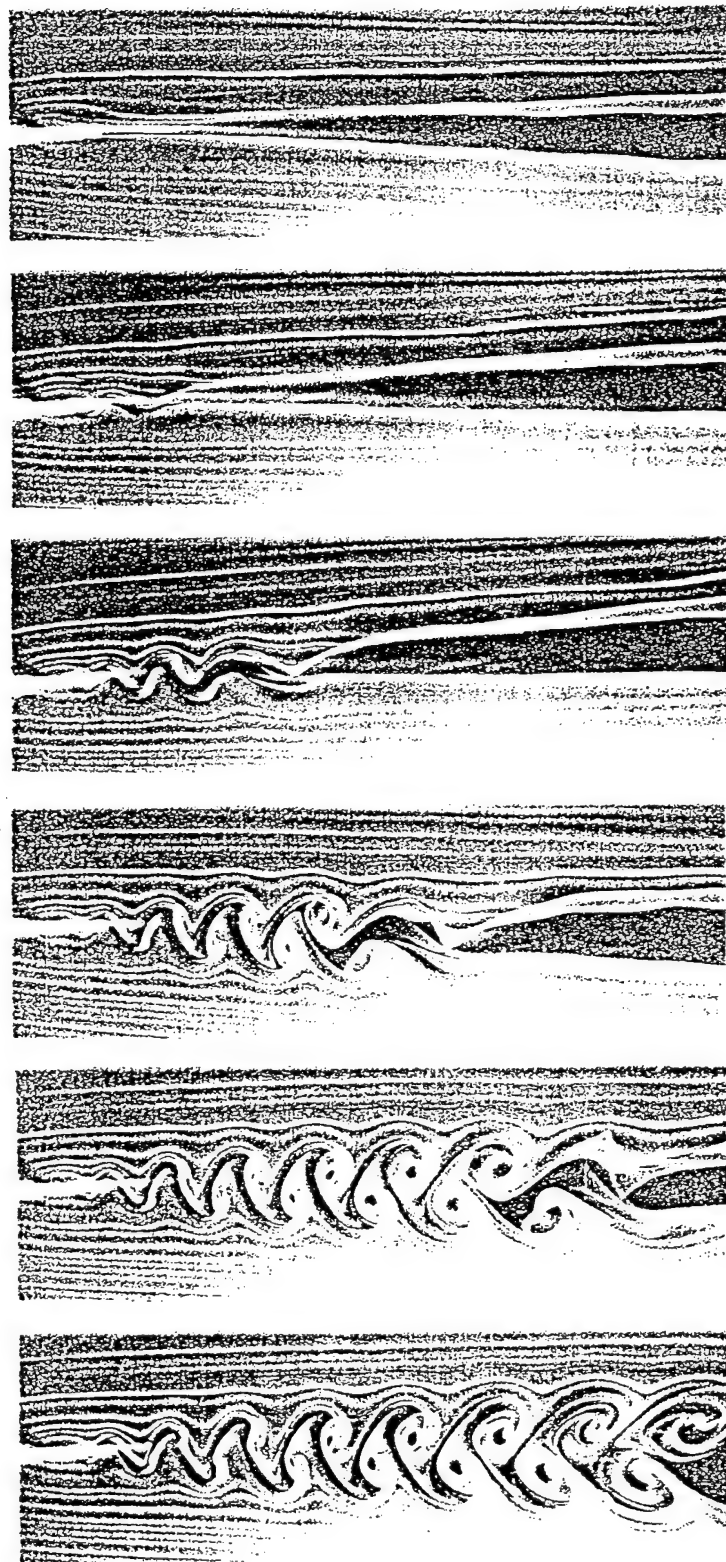
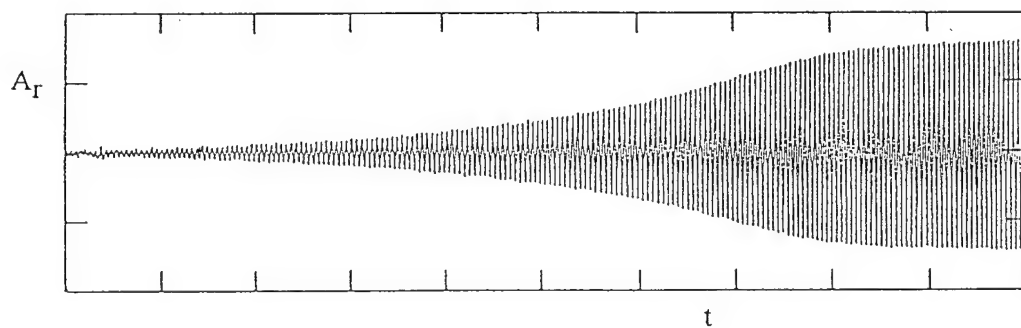(b) $c_{b,crit}$ R

Fig 1

Fig. 2

Fig. 3

$$\frac{\sigma_r D^2}{\nu}$$ (a) R_{crit}

$$\frac{\sigma_i D^2}{\nu}$$ (b) R_{crit}

$$\frac{l_i}{l_r}$$ (c)

Fig. 4

(a)

$(R-R_{cr}) / R_{cr}$

(b)

$|B| / |B|_{max}$

x / x_{max}

$R = 1.10\ R_{cr}$

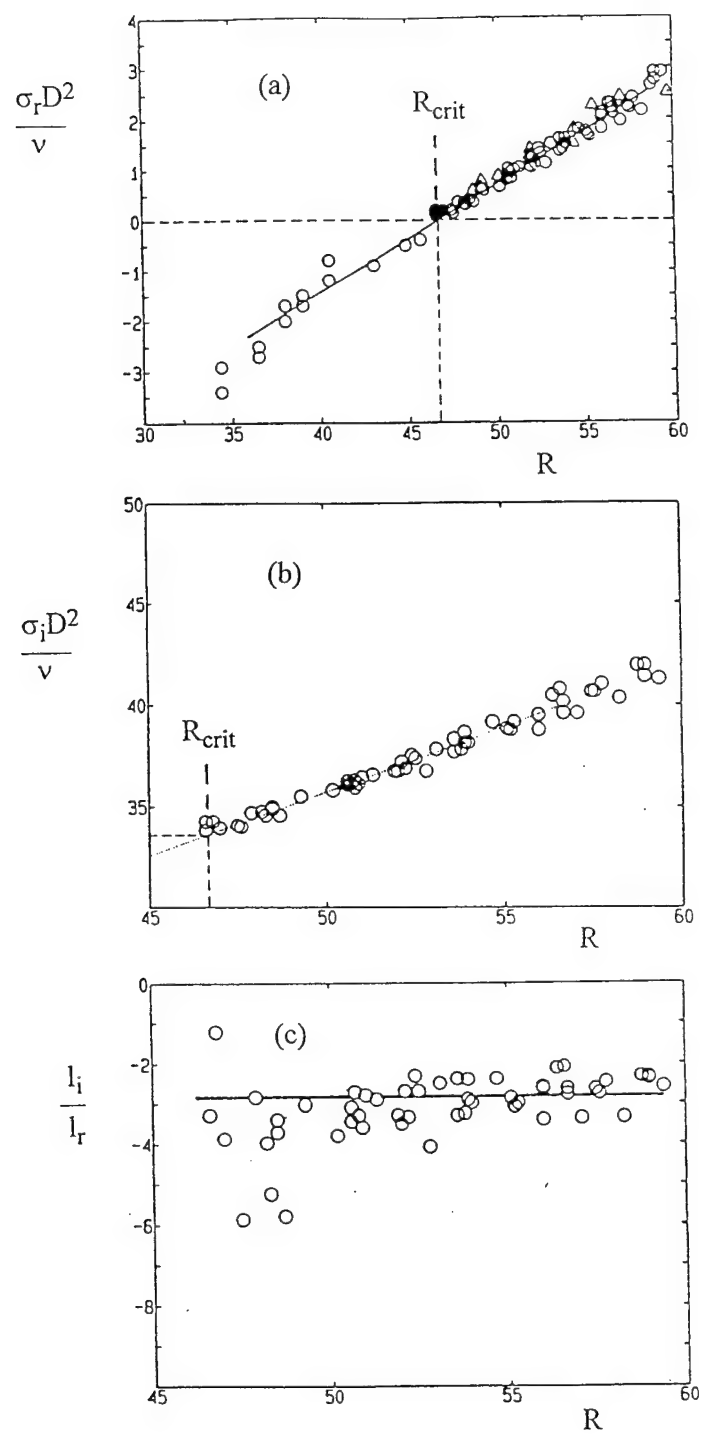$R = 1.16\ R_{cr}$
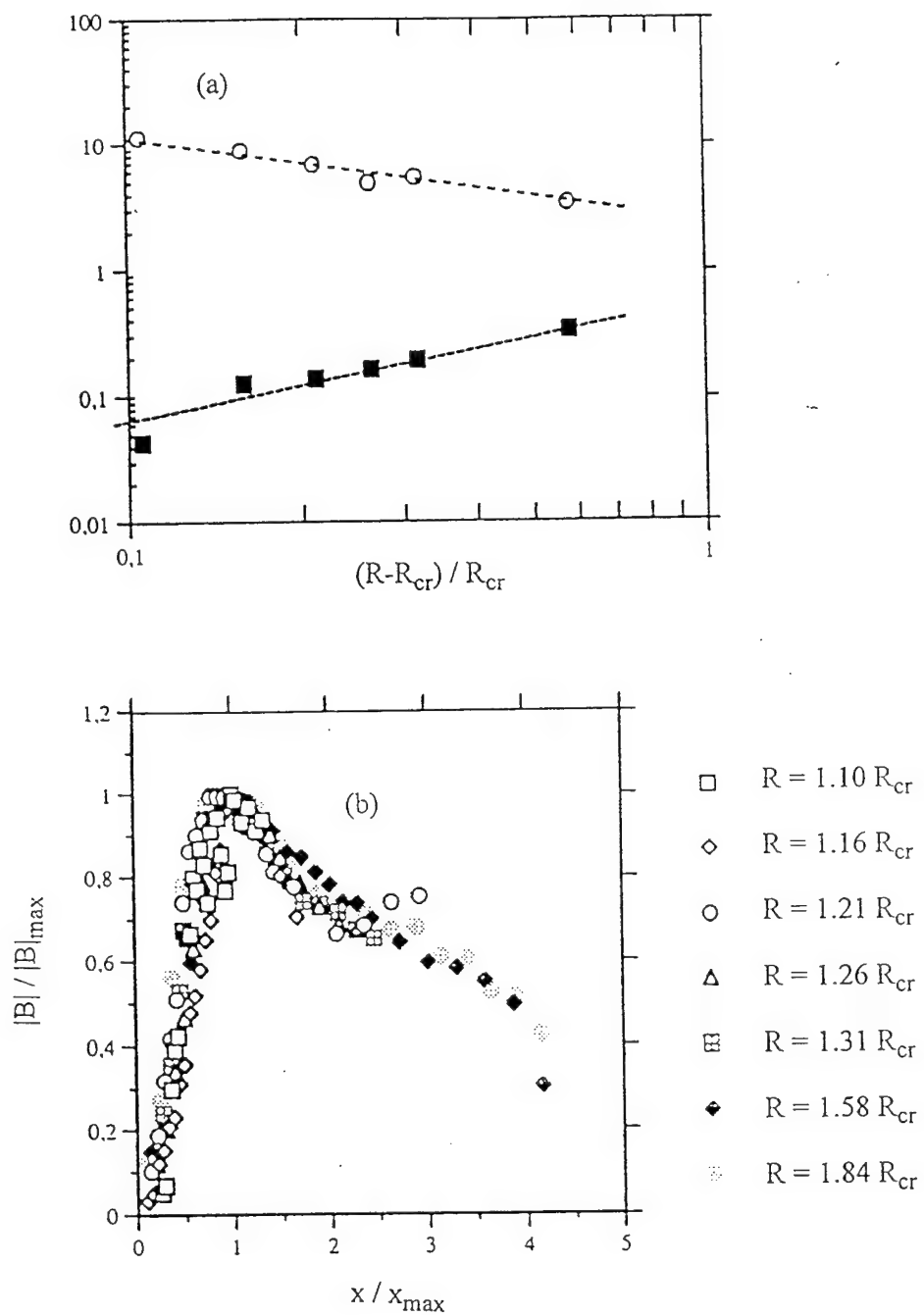
$R = 1.21\ R_{cr}$

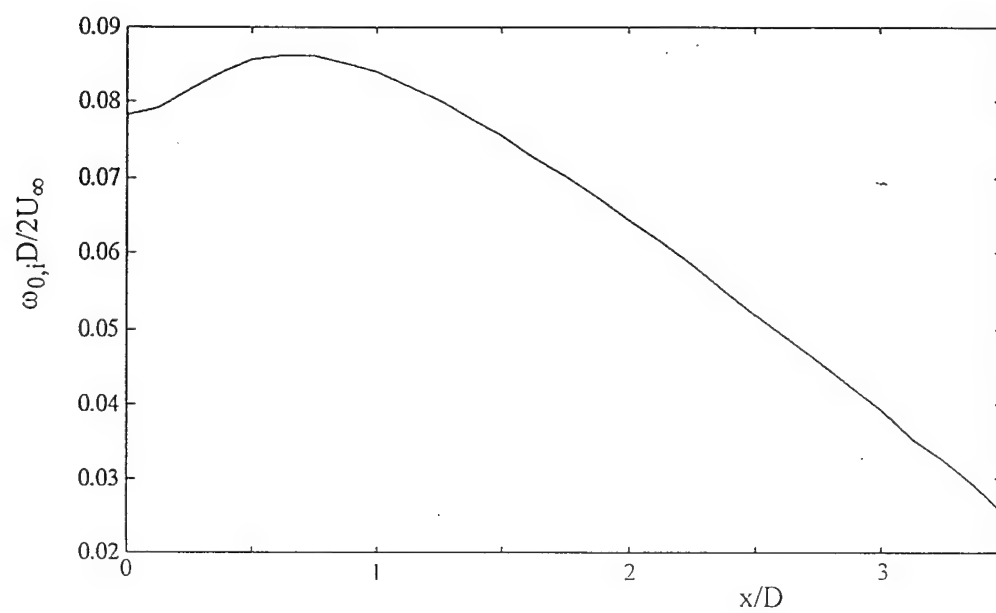$R = 1.26\ R_{cr}$

$R = 1.31\ R_{cr}$

$R = 1.58\ R_{cr}$

$R = 1.84\ R_{cr}$
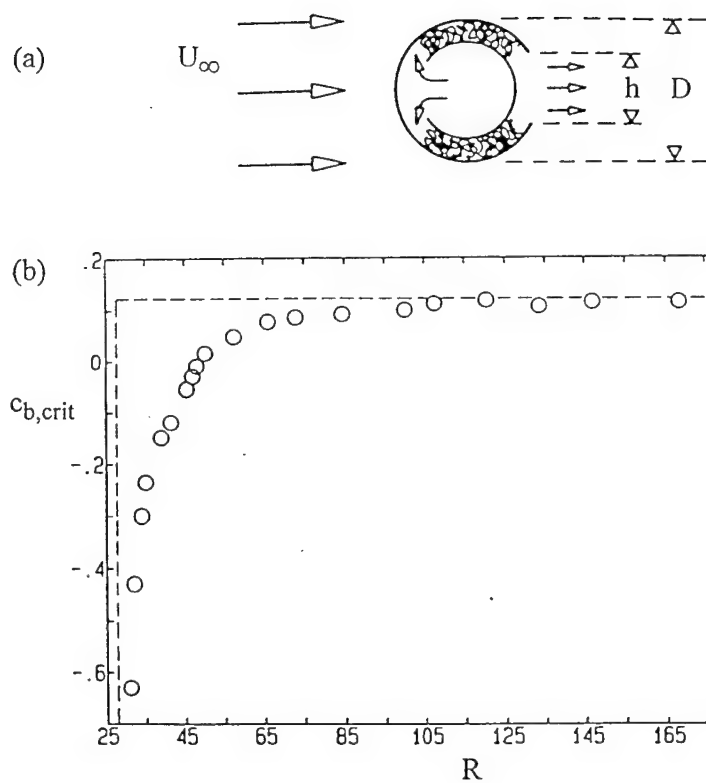
Fig. 5

Fig. 6
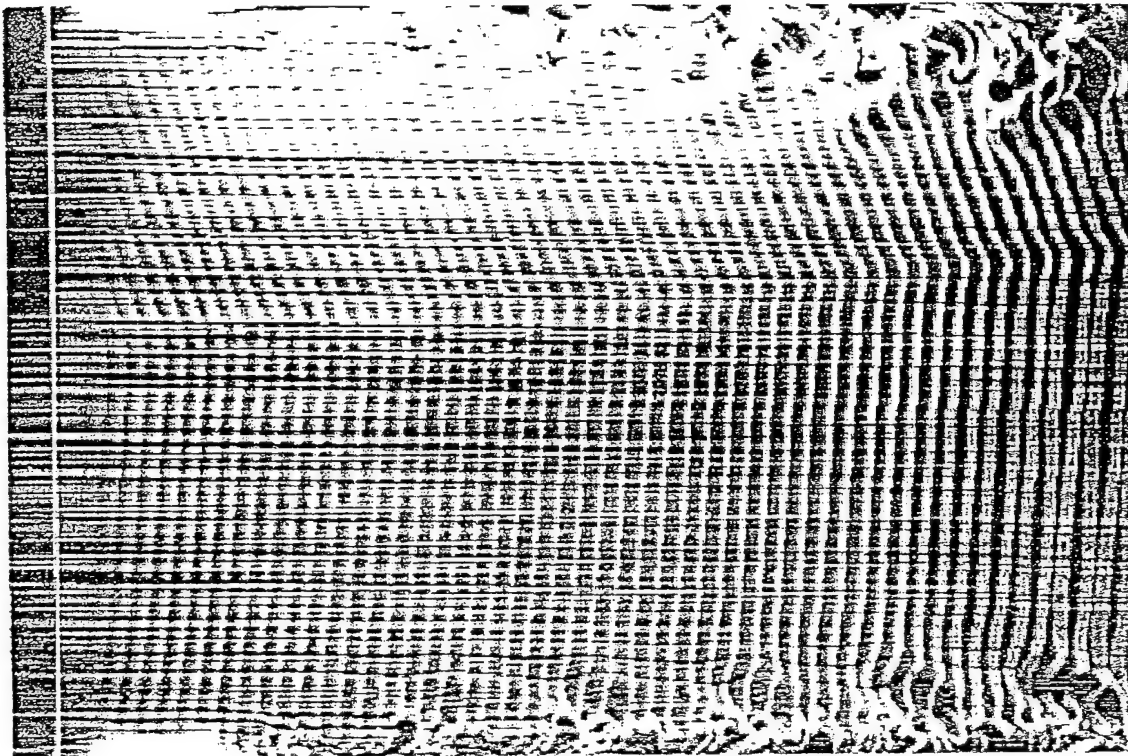
Fig. 7
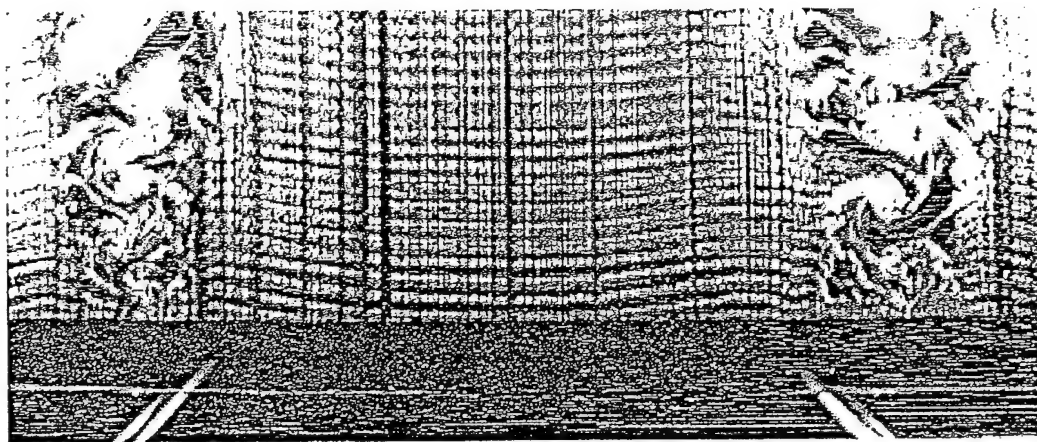
Fig. 8
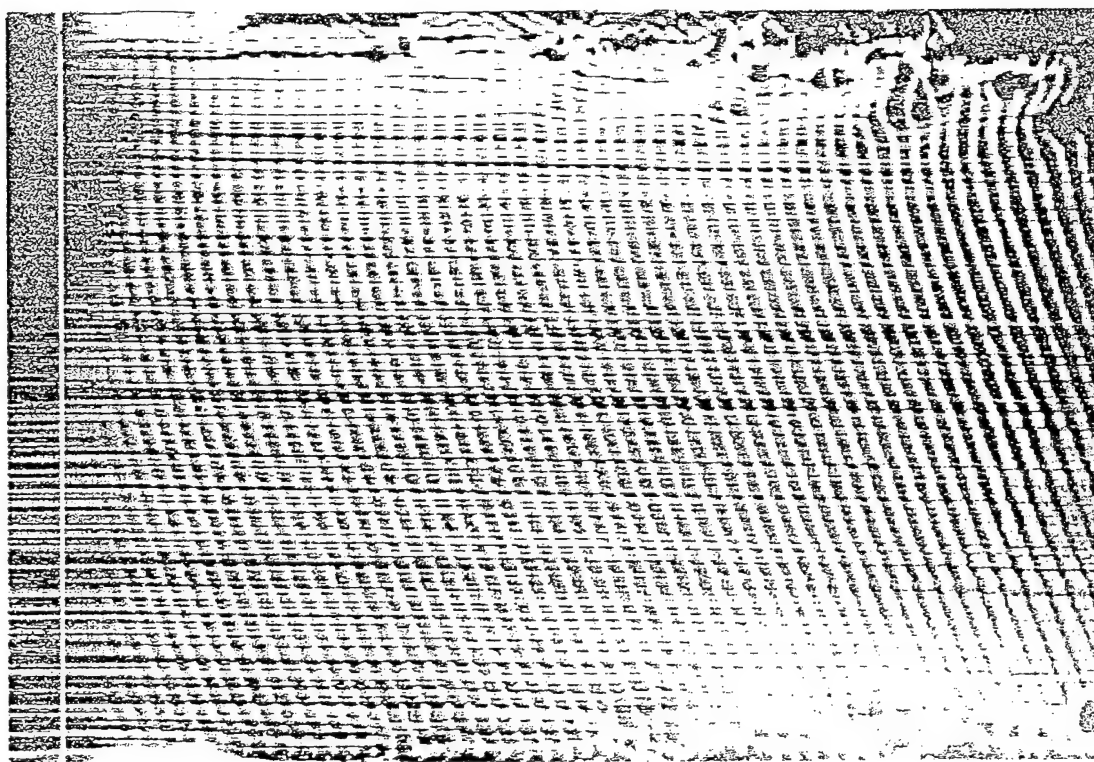
Fig. 9
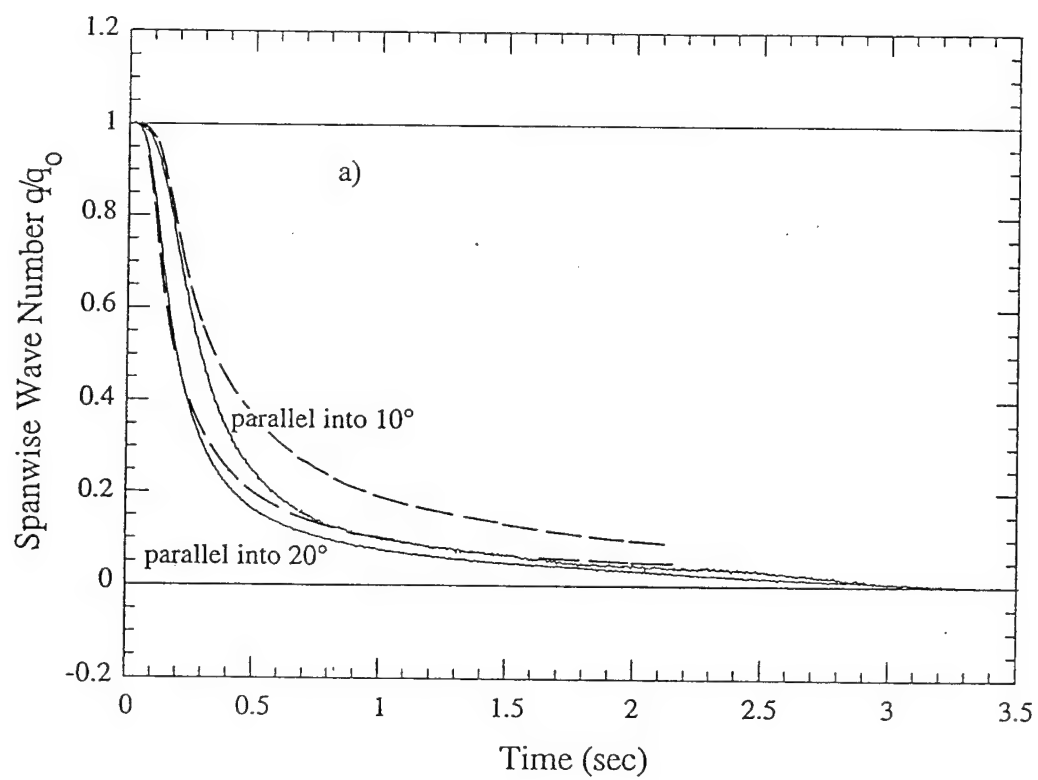
Fig. 10

III. THE DEVELOPMENT AND BREAKDOWN OF VORTICES ON A DELTA WING WITH 70° SWEEP AND FLAPS

Work performed by Wei Jun Fu

Abstract

Over a delta wing with 70 degree sweep angle, leading edge vortices form with increasing angle of attack. When the angle of attack α is smaller than 28 degree, the vortices are found to be stationary, due to the balance between the vorticity surface flux and the axial convection along the swept leading edge. When the angle of attack increases above 28 degree, the vortex breaks down. In this report, we investigate the development and breakdown of the leading edge vortices on a 70 degree swept delta wing with flaps. The flow visualization results show that the process of vortex formation and breakdown is highly sensitive to angle of attack α and flap angle ϕ. When the trailing edge flap is turned upwards (positive deflection angle), the vortex breakdown position moves forward with increasing flap angle. When the flap is deflected toward the pressure side of the wing (negative deflection angle), the vortex breakdown moves backward. Two flaps (trailing edge flap split at the centerline) appear to act independently on the two vortices, i.e. one vortex can be made to move forward and the other one backward if one of the flaps is deflected upward and the other one downward. Experiments with an external disturbance have also been performed at $\alpha=30°$ and $\phi=+5°$. We found in this case that the vortex breaks down immediately if an object touches the core of vortex. When the disturbance is removed, the vortex breakdown structure return promptly to its unperturbed position.

1. Introduction

Flow separation from the leading edge of delta wing gives rise to a spiral-like vortex sheet on the upper surface of the delta wing. Recent research [4-7] show details of the primary and secondary vortex system adjacent to the leading edge (see Fig.1). The consequence of the vortex pattern is to significantly increase the lift [1-3]. This attracts considerable interest because it can dramatically change the slope of the lift [8-10] (Fig.2). Some modern aircraft have already used delta wing designs to operate at high angle of attack. However, when the angle of attack is above some critical value, vortex breakdown may occur on the delta wing affecting the stability of the aircraft. Thus, the vortex breakdown phenomenon has become one tof today's active research topics.

Since the vortex breakdown location and its accompanying change in velocities cannot be measured with a probe without perturbing the natural flow field, flow visualization techniques are often used. By

injecting smoke into the flow upstream of the delta wing, the streamline with the vortex structure emanating from the leading edge can be easily seen.

In this report, the experimental setup is briefly described in section 2 and the salient features of vortex formation over the delta wing with sweep angle of 70 degree are shown in section 3. In section 4, we focus on the vortex breakdown. We investigate the influence of trailing edge flaps on the vortex breakdown in section 5. Finally, we study the influence of different flap deflection angles and of and external disturbances on the position of vortex breakdown in sections 6 and 7.

2. Experimental facility

The experimental setup is shown in fig. 3. The facility consisted of a wind tunnel with a delta wing, support system, laser, optical system, video recording system and smoke generator. The test section of the wind tunnel has a 1.2 meter by 1.0 meter rectangular cross section with a length of 1.5 meters. The maximum speed is 25 m/s. In this study, all the experiments were performed at 10 m/s. Fig. 4 shows the delta wing used in this study. It has a 70 degree sweep angle and a 26.6 degree sharp leading edge. The chord length L is 704mm and the wing span is 510mm. Two different length trailing edge flaps were used in the experiment. Their length l are 100mm and 170 mm, which make the ratio l / L equal to one seventh and one quarter respectively.

3. Distinguishing features of vortex formation

When the angle of attack α changes from 0 to 28 degree at a free stream velocity v=10 m/s, the vortex forms gradually and develops over the delta wing. In the beginning, the vortex does not separate until the angle of attack is greater than 4 degrees and remains attached to the top surface of the delta wing. When angle of attack is between 4 and 5 degree, the vortex begins to separate from the leading edge on the upper surface of the delta wing (see fig 5). Until the angle of attack reaches 28 degrees in fig. 6, a pair of steady separated vortices appear above the surface of the delta wing. The vorticity is generated at the leading edges and is wrapped up in the vortices. At the same time, a local shear layer begins to form (Didden and Ho 1986). In the experiment, we can see how the oncoming fluid first attaches to the lower surface near the leading edge of the delta wing. Due to the favorable pressure gradient in the direction towards the edge, the flow stays attached to the bevel of the leading edge and only separates from the sharp L.E. to form a concentrated vortex. The vorticity in the shear layer is wrapped up in spiral fashion into large bound vortical structures that are convected downstream with the velocity of the free stream. The vorticity generated at the leading edge is carried downstream by the velocity component along the inclined leading edges and when the vorticity supplied from the L.E. balances the vorticity convected away, the separation vortices become stationary [11-12]. The two vortices above the suction surface of the wing have a conical symmetry with respect to the apex of the lifting surface.

The low pressure associated with the vortices induces additional lift on the wing, often called nonlinear vortex lift, which is particularly important at large angle of attack [13].

4. Survey of vortex breakdown research

Now, let us look at the results for angles of attack increasing from 28 to 55 degree. When the angle of attack is greater than 28 degree vortex breakdown will first appear on the delta wing near the trailing edge and the vortex breakdown location "B" moves forward with increasing angle of attack (fig.7 & 8). With further increasing angle of attack, the velocity on the suction side decreases and the downstream convection of vorticity is reduced thus changing the balance of vorticity. Eventually the leading edge vortices can not be held in place and shed. At intermediate angles of attack, a adverse streamwise pressure gradient builds up as α increases and at angles of attack beyond 28 degrees the vortices suddenly expand in size accompanied by a decrease in axial velocity, i.e. they burst . This is often accompanied by transition where the organized vortex structure breaks down into turbulence. For α equal to 50 degrees, point "B" has moved close to the apex of the delta wing. This picture is consistent with Parmenter's study [16] who applied suction near the trailing edge, thereby effectively lowering the adverse pressure gradient. By lowering the adverse gradient, the tendency to vortex breakdown is reduced just as in the case of boundary layer separation [10]. The location of the suction probe and the suction rate determine the effect of suction on vortex breakdown. Parmenter determined that the location of the suction device must be located downstream of the natural vortex breakdown point (see also the theoretical studies by Benjamin [17-18]). In figure 9 the effect of breakdown on the visualization of vortex sections is shown. The sudden increase of the the central smoke-free inner core is striking and permits an accurate visual determination of the breakdown location.

5. Vortex breakdown on a delta wing with trailing edge flap

For this experiment, we use two angles of attack 28.5 and 30 degree with different flap deflection angles equal to 35, 10, 5, 0, -5 and -10 degrees to investigate the influence of the flap on the delta vortices. For example, for an angle of attack of 28 degrees and a free stream velocity v of 10 m/s, the results demonstrate that the position of vortex breakdown moves from the trailing edge to the apex in fig 10. When the flap deflection angle increases from 0 to 30 degree, the core line on the top of the delta wing is gradually lifted with increasing flap deflection angle. Conversely, the position of vortex breakdown moves downstream and off the upper surface of delta wing, when the flap deflection angle is increased in the negative direction. We also oscillated the flap at different frequencies and amplitudes (45°to -20° or 0° to 30°). The results show that the position of vortex breakdown moves forward and backward corresponding to the flap up and down phase of oscillation. The phase of the vortex breakdown motion is very well synchronized with the flap motion at low frequency and confirms the

strong sensitivity of the breakdown to streamwise pressure gradient. If the flap is deflected upward, the local pressure gradient changes on the back of upper surface of the delta wing. The increased adverse pressure gradient makes the position of vortex breakdown move forward and conversely, when the flap is deflected downward, the local pressure gradient is reduced and causes the position of breakdown to move back. This is illustrated by figure 12 which shows wall streamlines on the top side of the delta wing without and with flap. It is noted that breakdown is associated with a "dislocation" (an inward bow) of the otherwise perfectly straight separation line thus providing another means of nonintrusively locating the breakdown position.

6. Effect of different flap angles on left & right half wing

The influence of different flap deflection angles, ϕ_L and ϕ_R, on the left and right half of the wing trailing edge was investigated. In this experiment, four combinations of different angles are used which are shown in Fig 11. The results of experiment show that, when $\phi_L > 0$ the position of breakdown of the left vortex moves forward. When $\phi_R < 0$, the position of breakdown of the right vortex moves backward. At the same time, the left core and right core lines independently lift from and approach the surface of the delta wing.

7. External disturbance of vortex

For α equal to 30 degrees and a flap deflection angle of 5 degrees, the vortex was disturbed from the outside by poking a thin steel thread ($\varnothing=0.5$ mm) or a rod ($\varnothing=2$ mm) into the vortex core. Fig. 13 shows schematically the influence on the breakdown location. When the steel thread is outside of the vortex core, the breakdown structure doesn't show any significant change, but if the steel rod touches the vortex core upstream of the unperturbed breakdown point, vortex breakdown immediately occurs at the rod location. When the disturbance is removed, the vortex promptly returns to its usual position. Each vortex is found to react independently without affecting the other vortex. These results show that when an object directly disturbs the vortex core by introducing a local stagnation region, vortex breakdown immediately occurs at the disturbance point. As the vortex core contains high momentum fluid with high velocity and low pressure (see the figure by Fink and Taylor, 1967, reproduced as fig. 14), the observed reaction to the insertion of a rod is as expected.

8. Conclusions

Flow visualization has documented the vortex formation process, the change of breakdown position of the separation vortex when the angle of attack was increased beyond 28.5 degrees and the final disappearance of the steady delta vortices. Vortex breakdown position on the delta wing has been found to move upstream or downstream when the flap was deflected up or down. Different flap deflection

angles both left and right allowed to move the vortex breakdown position of each vortex independently in different directions and has demonstrated that the burst position is extremely sensitive to angle of attack and flap deflection angle. Flow visualization also revealed that when a rather thin solid object directly disturbs the core of the vortex, it immediately bursts at the disturbance position.

References

1. Lee, G. H.," Note on the Flow Past Delta Wing with Sharp Leading Edges," Aeronautical Research Council, Rept. and Memorandum 3070, sept. 1958

2. Ornberg, H., " A Note on the Flow Around Delta Wing," Swedish TNK. T.H. Aero. TN 38. 1954

3. Elle, B.J., "An Investigation at Low Speed of the Flow Near the Apex of Delta Wings with Sharp Leading Edges," Aernautical Research Council, Rept. and Memorandum 3176, 1958

4. Kuechemann, D., " The Aerodynamic Design of Aircraft - An Introduction, Pt. V." Royal Airforce Establishment TM 1622, 1975.

5. Hoeijmakers, H. W. M., " Computational Vortex Flow Aerodynamics," Aerodynamics of Vortical Type Flows in Three Dimensions," AGARD CP 342, 1983, pp. 18.1-18.35.

6. Rizzi, A., Eriksson, L. E., Schmidt S., " Numerical solutions of the Euler Equation simulating Vortex Flow Around Wing," Aerodynamics of Vortical Type Flows in Three Dimention, AGARD CP 342, 1983, pp. 21.1-21.14.

7. Woodon S. H. and Dejarnette, R., "A direct and Inverse Boundary Method for subsonic Flow over Delta Wing," Vortex Flow Aerodynamic, NASA Conference Publication. 241, Vol. 1. edited by J. F. Campbell, R. S. Osborn, and J. T. Foughner, 1986, pp. 115-134.

3. Peckham, D. H. and Atdinon, S. A., " Preliminary Result of Low Speed Wind Tunnel Test on a Gothic Wing of Aspect Ratio 1.0, " Aeronautical Research Council, CP 518, 1957

9. Earnhshaw, P. B. and Lawford, J. A., "Low-speed Wind Tunnel Experiments on a Series of Sharp-edged Delta Wings," Aeronautical Research Council, R & M 3424, 1966.

10. Hummel, D. and Srinivasan, P. S., " Vortex Breakdown Effects on the Low-speed Aerodynamic Characteristics of Slender Delta Wings in Symmetrical Flow," Journal of the Royal Aeronautical Society, Vol. 71, 1967, pp. 319-322.

11. Sidney Leibovich, " Vortex Stability and Breakdown: Survey and Extension," AIAA JOURNAL, Vol. 22, No. 9, 1983, pp 1192-1193.

12. Mario Lee and Chih-Ming Ho, " Lift Force of Delta Wing," Applied Mechanics Reviews Vol. 43, No. 9, September 1990. pp 209.

13. Mohamed Gad-el-Hak, "Control of the Discrete Vortices from a Delta Wing," AIAA JOURNAL Vol. 25, No. 1, 1986, pp 1042-1043.

14. Wentz, W. H., Jr. and Kohlman, D. L., " Wind Tunnel Investigations of Vortex Breakdown on Slender Sharp-Edged Wings," NASA CR-98737, Nov. 1968.

15. Faery, H. F. Jr., Trozier, J. K., and Ham, J. A., " Experimental and Theoretical Study of Three Interacting, Closely-Spaced, Sharp-Edged 60 Delta Wings at Low Speeds," NASA CR-3460, 1981.

16. Parmenter, K. and Rockwell, D., " Transient Response of Leading Edge Vortices to Localized Suction," AIAA Journal, Vol. 28, Number 1, March 1990.

17. Benjamin, T. B., "Theory of the Vortex Breakdown Phenomenon," Journal of Fluid Mechanics, Vol. 14, June 1962.

18. C. E. Synolakis, B. D. Breuel, M. Tegulapalle, C. M. Ho, "Passive Control of Delta Wing Rock," Journal of Aircraft, Vol. 30, Number 1, 1993, pp. 131-133.
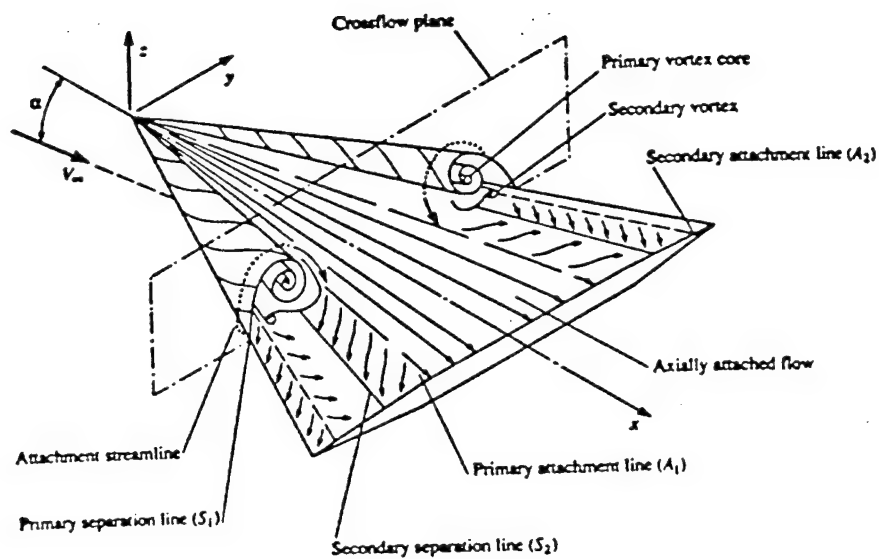
Fig. 1   Diagram showing the vortex flow field over
the upper surface of a delta wing. (from
Anderson,J.,Fundamentals of Aerodynamics,
McGraw-Hill, New York,1991)
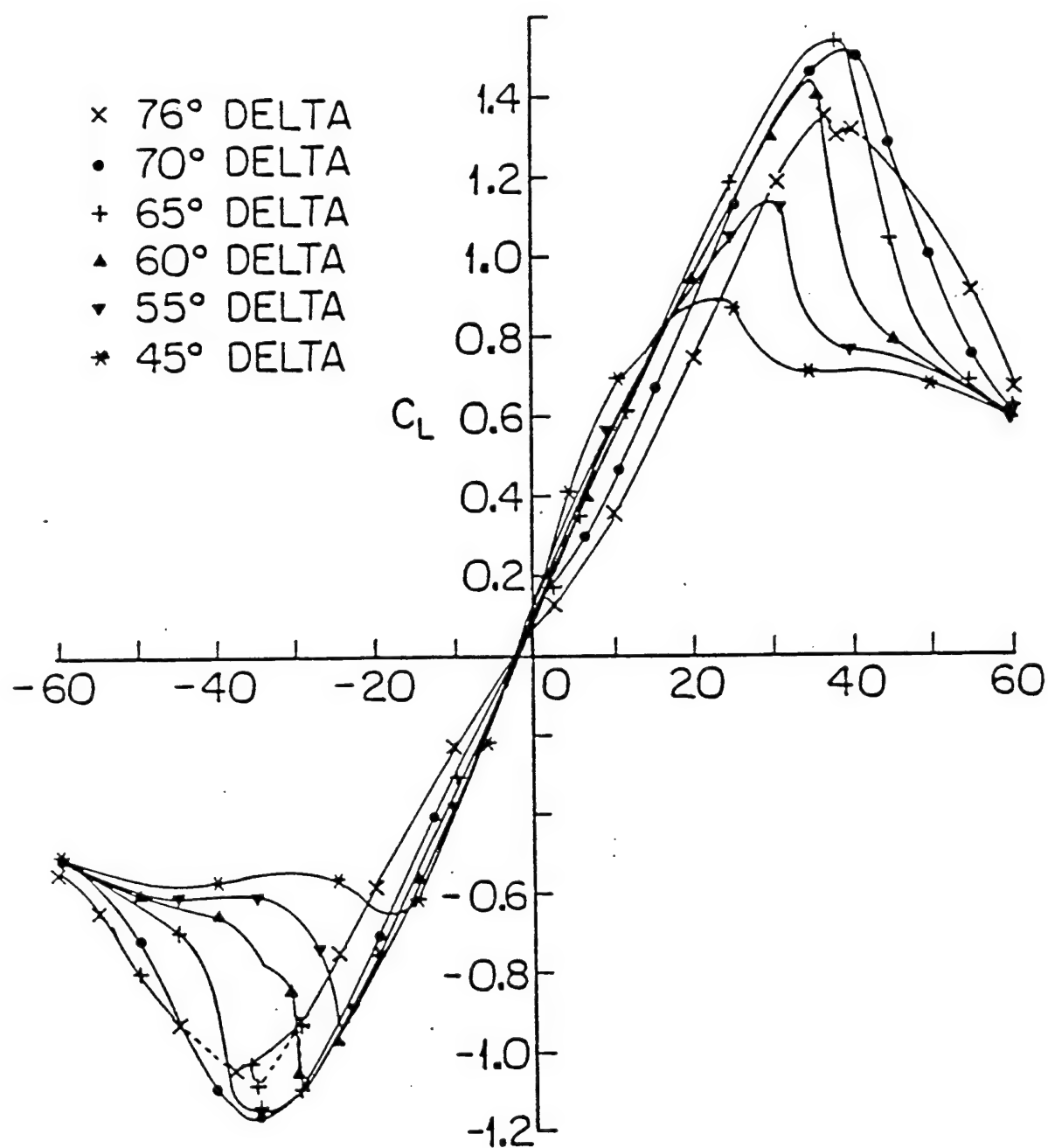
Fig. 2   Lift coefficient with angle of attack,Earnshaw
          and Lawford[1964]
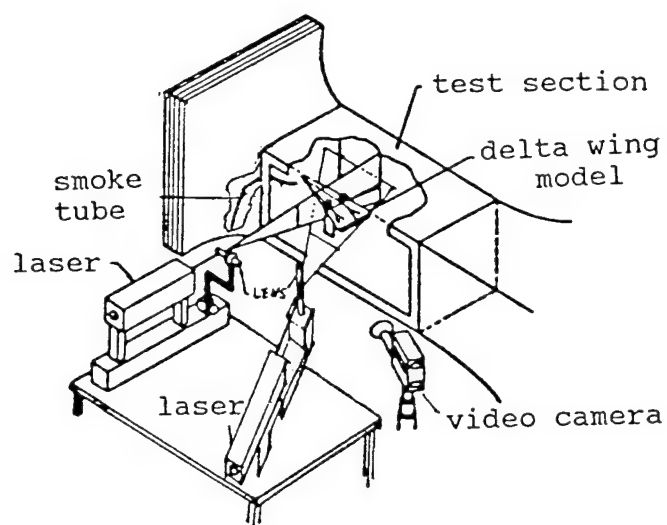
Fig. 3   Experimental facility
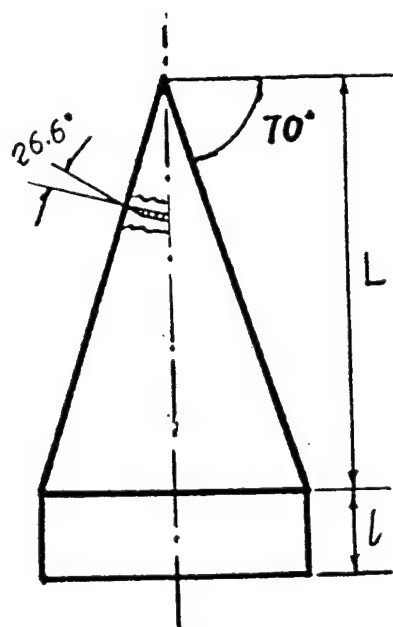
Fig. 4   Delta wing model and simulate flap
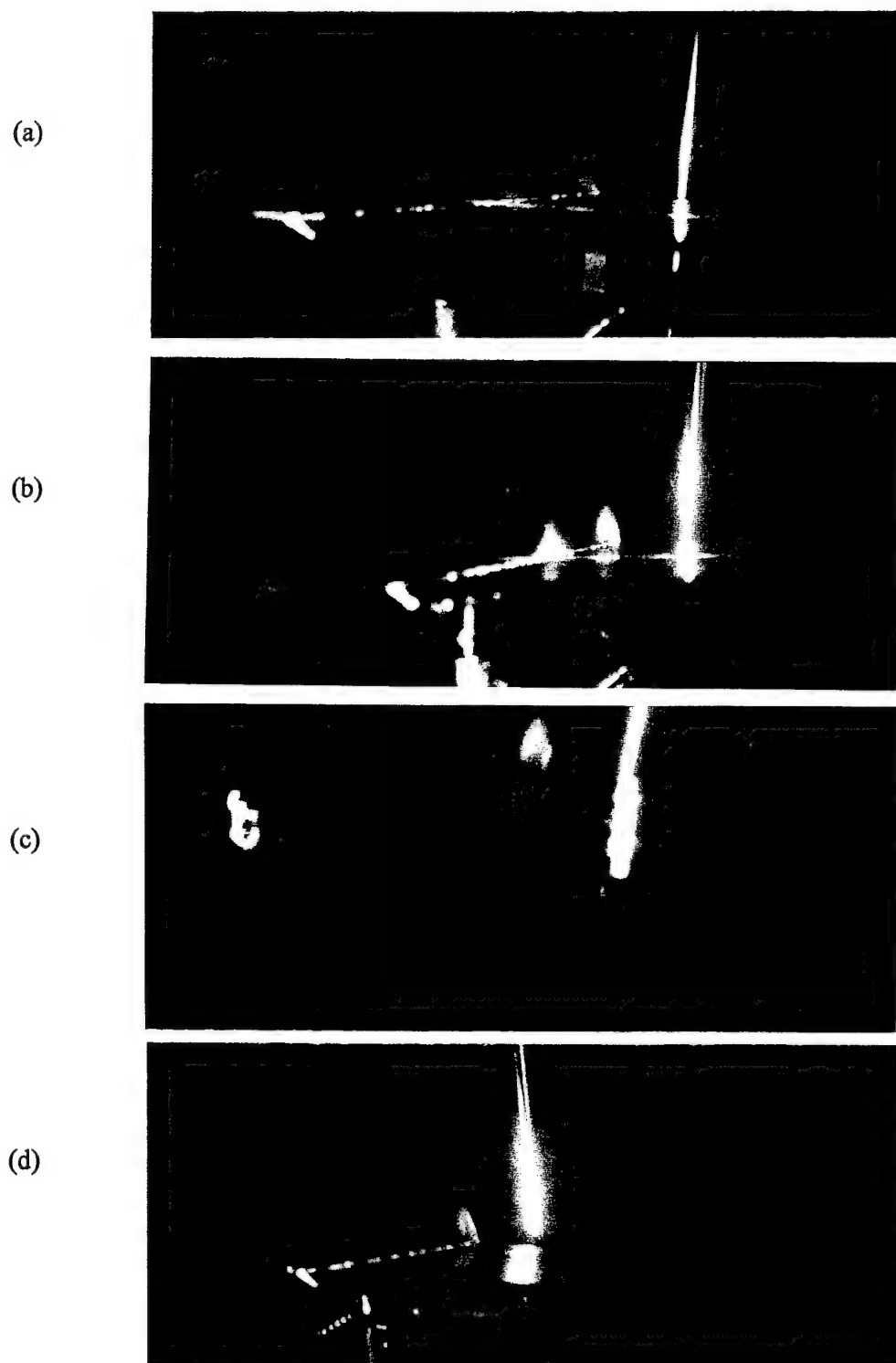
Fig. 5   Visualization of the vortex formation stage at small angles of attack.
             (a) $\alpha=2°$; (b) $\alpha=3°$; (c) $\alpha=4°$; (d) $\alpha=5°$.
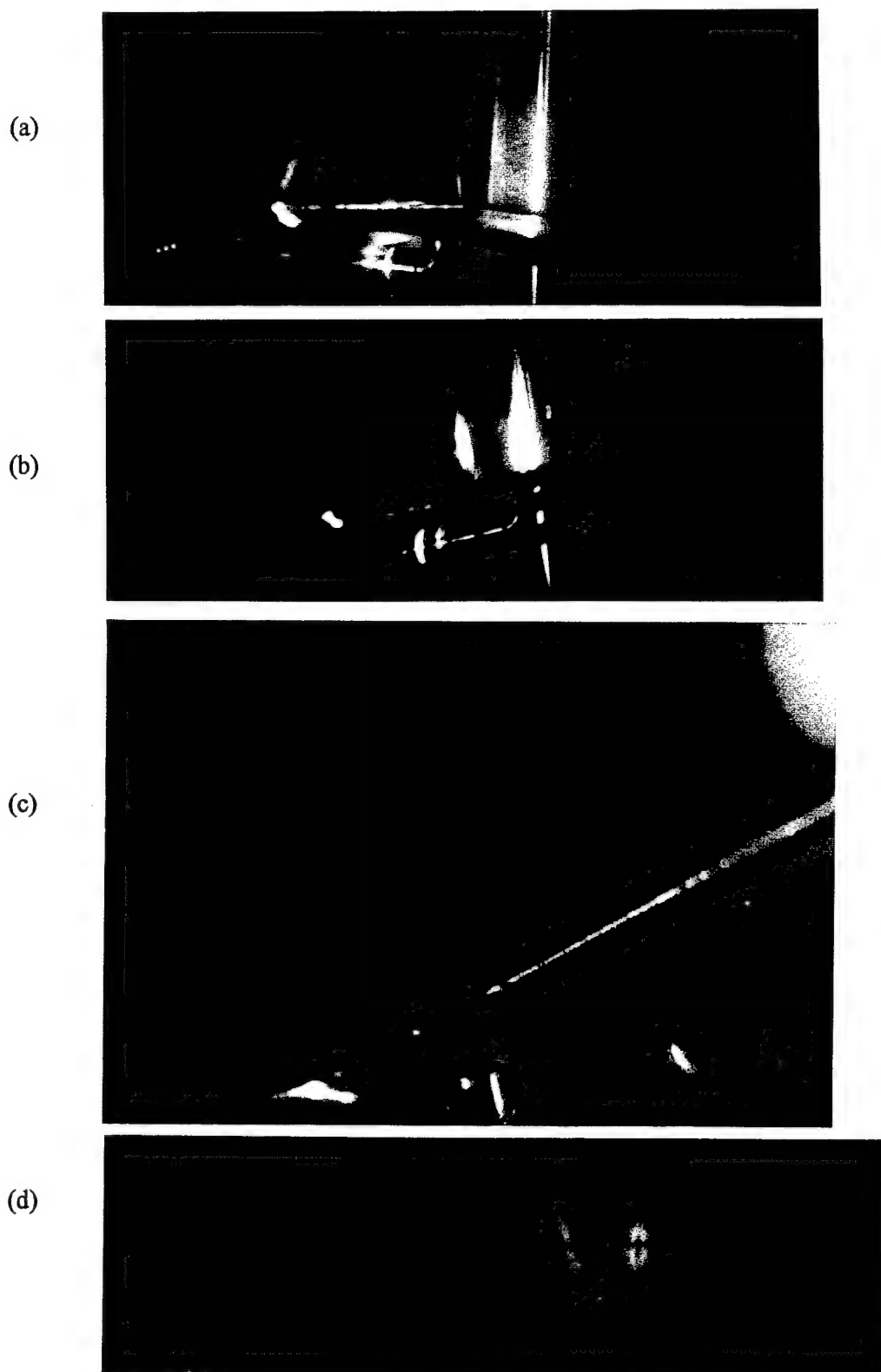
Fig. 6   Visualization of fully formed delta vortex. (a) section with α=10°;
(b) section with α=20°; (c) two consecutive sections with α=25°; (d) cut
along the core with α=25°.

(a)

(b)
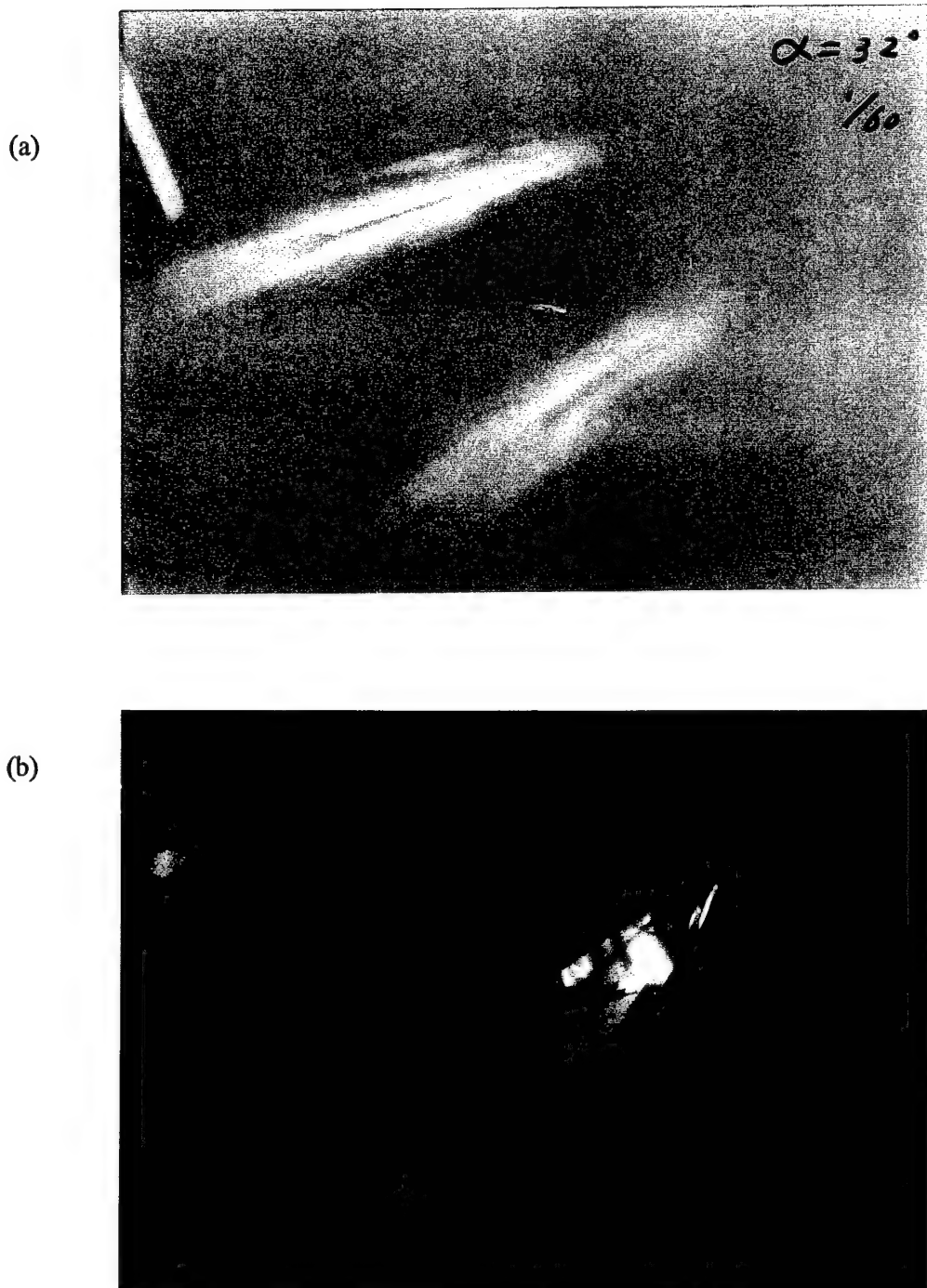
Fig. 7   Laser cuts through the vortex core with breakdown structure. (a) α=32°;
(b) α=40°.
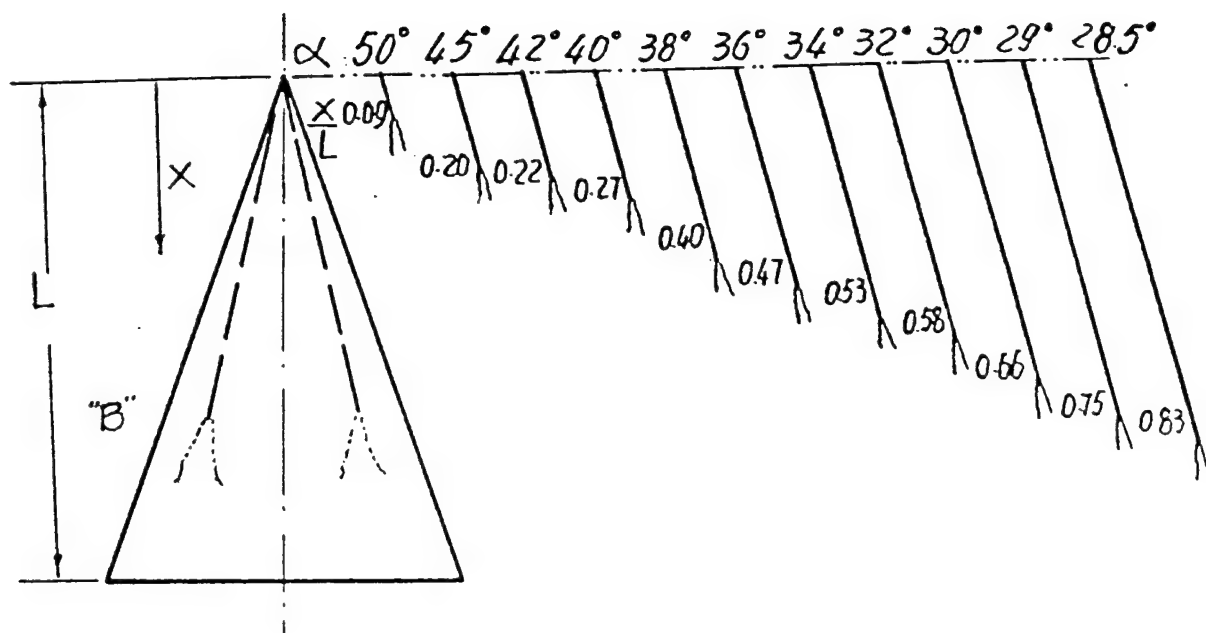
Fig. 8   Change of vortex breakdown position x/L with angle of attack. Core centerlines and breakdown structures are shown schematically on the right of the wing
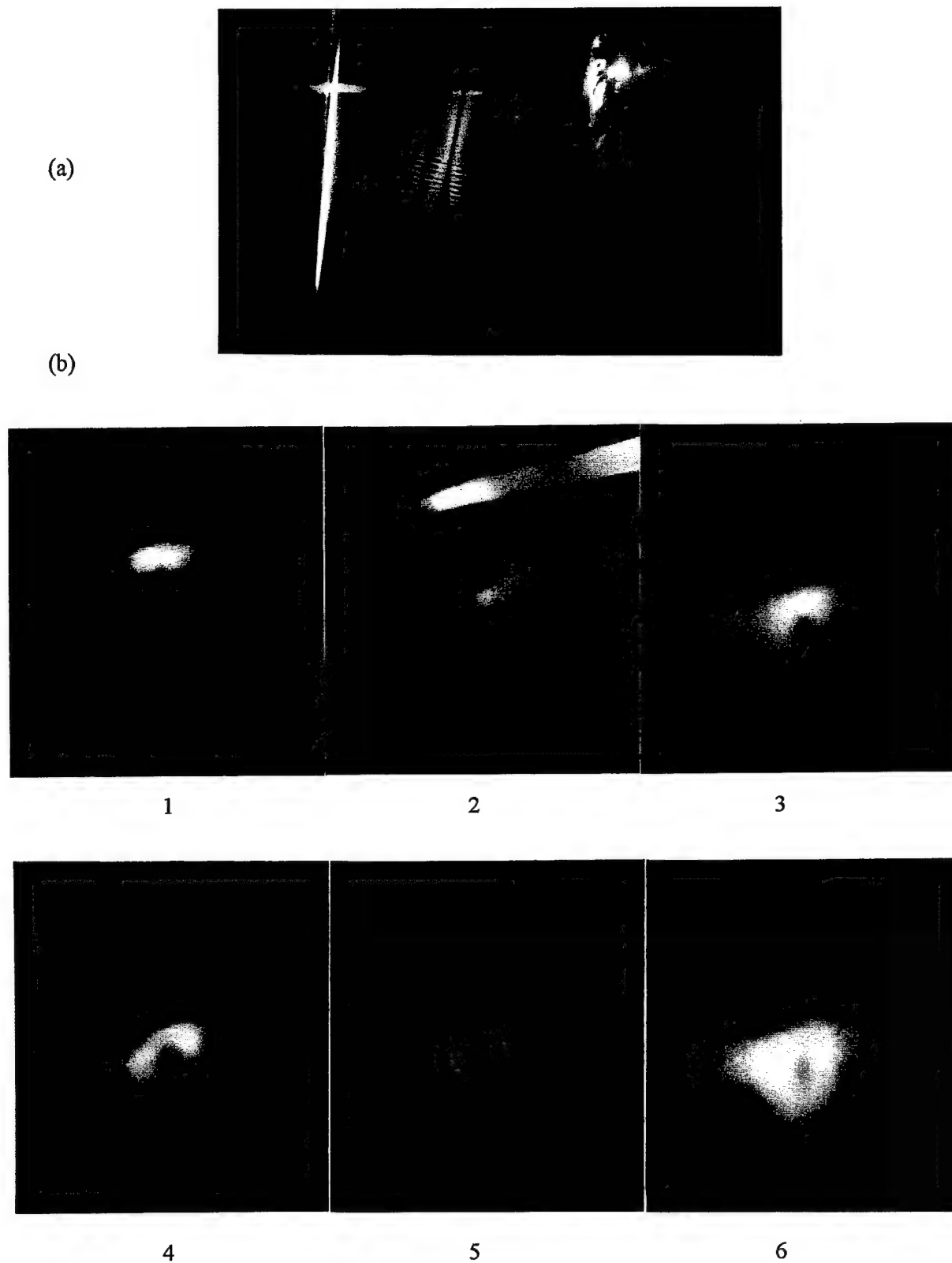
Fig. 9   Cross sections of vortex around the breakdown location. (a) definition of section numbers on a streamwise cut. (b) sections 1-6 showing the rapid increase of the diameter of the smoke-free "bubble."
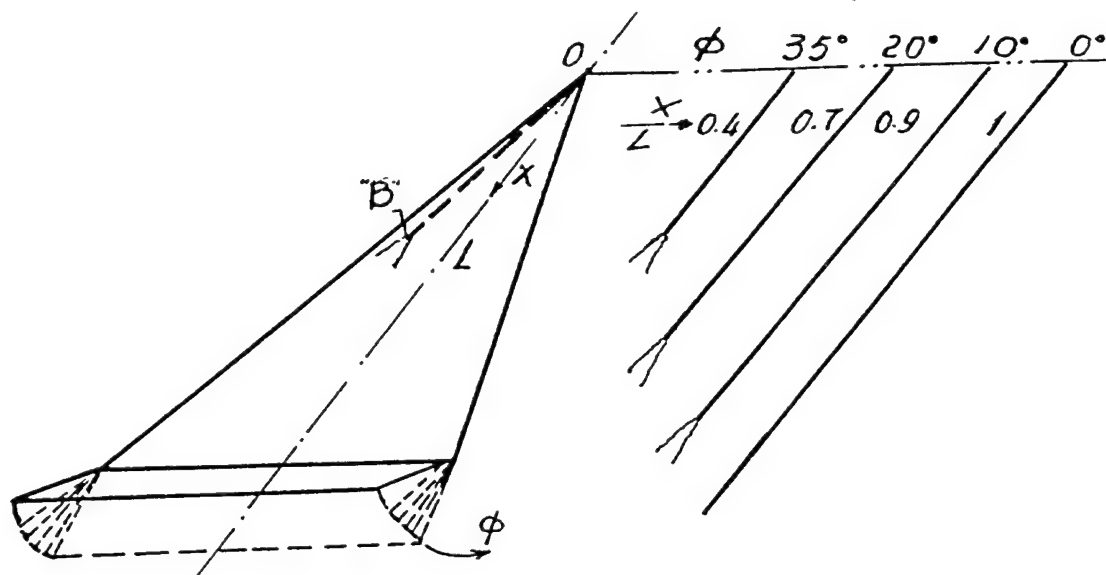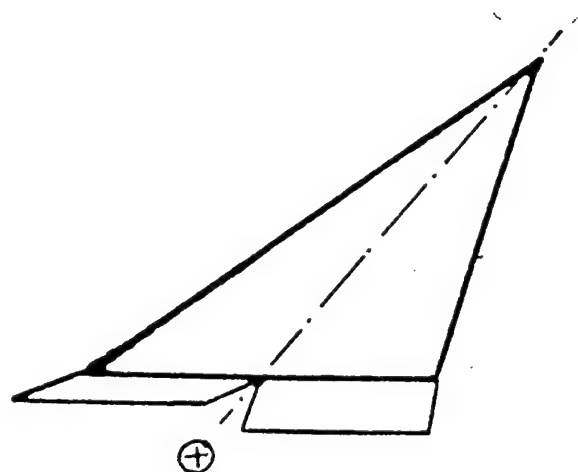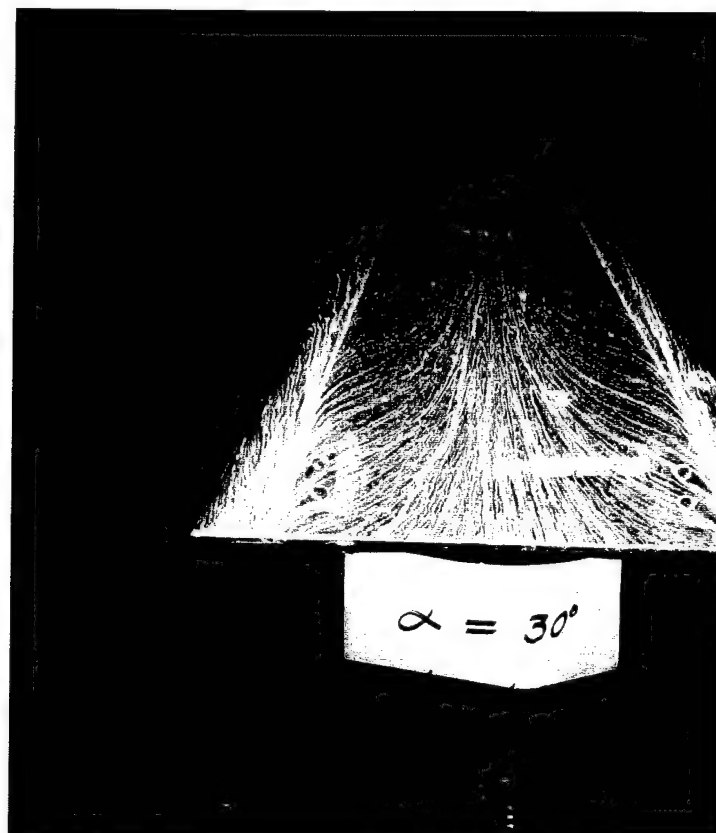
Fig. 10   Breakdown position change with flap deflection
            angle   on the delta wing schematic diagram
            (left   coreline of vortex as example)

	ϕ_L +	— ϕ_R
1	+ 5	- 5
2	- 5	+ 5
3	- 10	+ 10
4	+ 5	+ 10

Fig. 11   Different flap deflection angle ϕ_L & ϕ_R
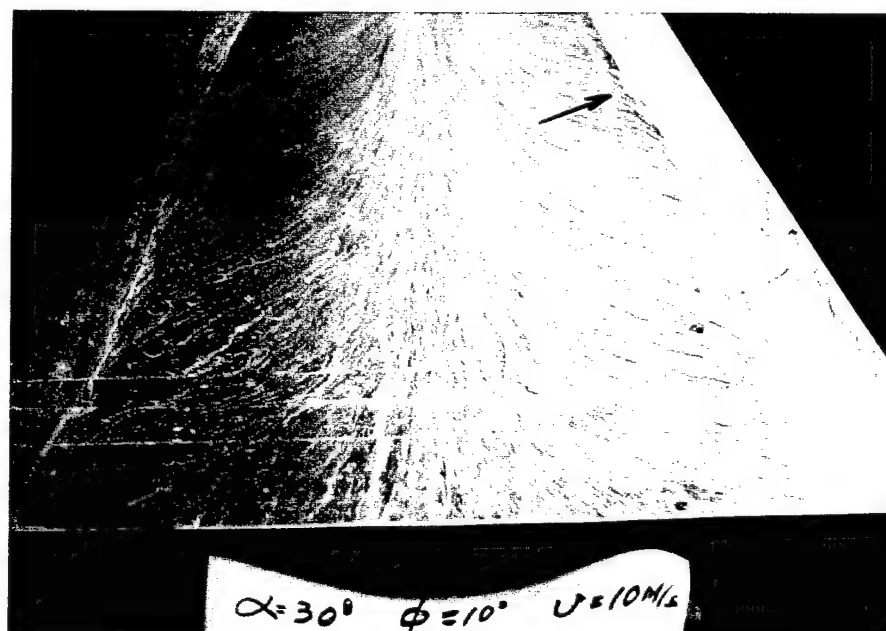   schematic diagram (a=28° l/L=1/4)

Fig. 12   Wall streamlines on top surface of delta wing at 30° angle of attack. (a) no flap. (b) flap at +10° ; vortex breakdown has moved upstream and causes a clear "dislocation" of the separation line.
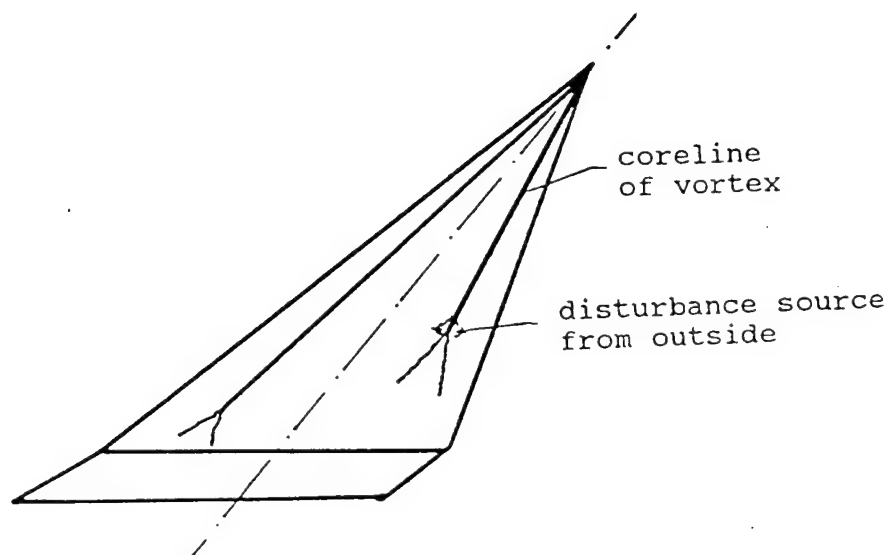
Fig. 13   Effect of additional external disturbance on vortex breakdown location.
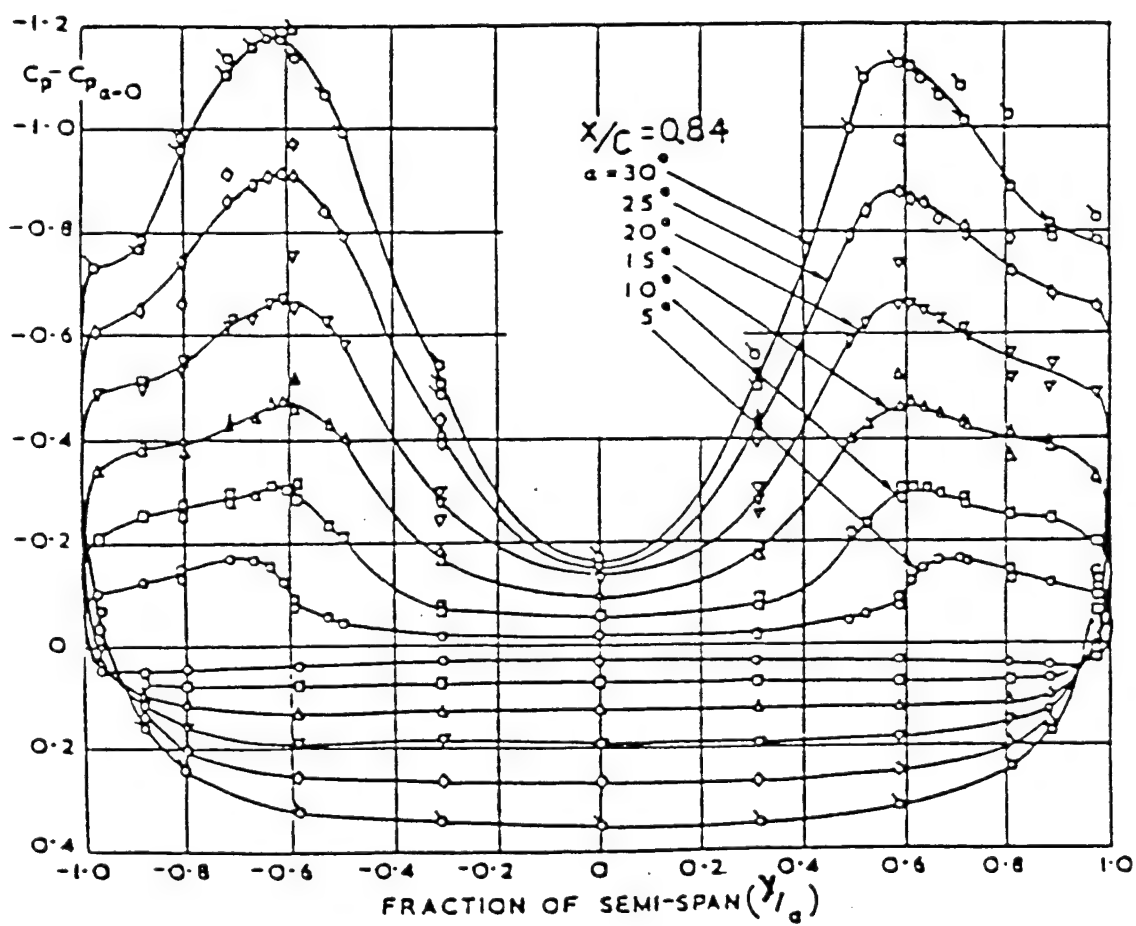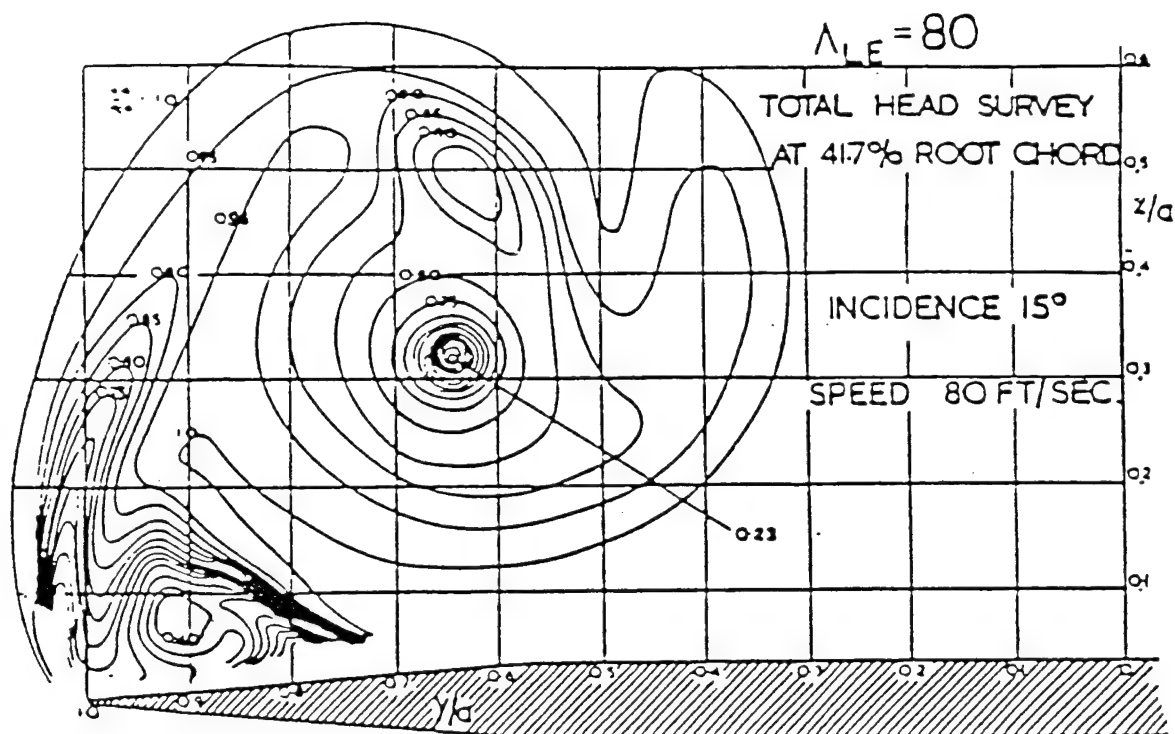$\alpha = 30°$, flap angle $\phi = +5°$.

Fig. 14   (a) Total head distribution in a section perpendicular to the L.E. vortex.
(b) Corresponding surface pressure [from Fink & Taylor, 1967] .

IV. LINEAR CONVECTIVE AND ABSOLUTE INSTABILITY OF IDEALIZED COLUMNAR VORTICES

work performed by M. Z. Pesenson

The cores of columnar vortices exhibit, under some conditions, a rapid change to a rather different flow state. This phenomenon is called vorlex breakdown or vortex bursting, as the core appears to burst or increase its size in a distance of order R (R being the core diameter) [1]. The possibility of breakdown is a remarkable feature of the behavior of vortex cores. Since Peckhman & Atkinson [2] drew attention to it in flow over wings with highly swept leading edges at large angles of incidence, the phenomennn has been studied intensiveely both experimentally and theoretically [3-7].

The center of a leading-edge vortex is, for moderate angles of attack, located on the order of a core diameter above the wing surface, where the core diameter may not be negligibly small compared to the local semispan of the wing. During vortex breakdown the core diameter increases substantially, leading generally to unsteady loading of the delta wing as the breakdown location is very sensitive to small disturbances of flight conditions [8]. The phenomenon of vortex breakdown has also favorable effects in combustion chambers, where it is used as "flameholder," in tornado funnels, etc.. The bursting has recently also been observed experimentally [9] in concentrated vortex filaments within a turbulent flow and may therefore be an agent in the generation of the small scales in high Reynolds number turbulence.

Despite numerous analytic and experimenlal attempts, which are summarized in many reviews, the explanation of the mechanism giving rise to the vortex breakdown has remained a source of controversy. In this study we report a new approach to the vortex stability problem which illuminates its absolute versus convective instability characteristics [10]. It allows us to interpret experimental observations of oscillations in the wake of vortex breakdown structures and leads, at the same time, to a complex group velocity criterion for the breakdown of vortex flow.

Most of the theoretical approaches to the vortex breakdown problem fall into the following three classes:

- Theories focussing on the deceleration of the axial core flow, leading to a stagnation point on the axis [11];
- The concept of critical state [12];
- Hydrodynamic instability analyses [13,14].

An important point was made by Saffman [1] who pointed out that there is a close connection between vortex breakdown and the existence and uniqueness of solutions to the steady incompressible Euler equations. However, the connection between the first class of theories and

Saffman's results on the one hand and vortex breakdown of spatially and temporally evolving vortices is not yet clear. We also note that the critical state approch is based on the behavior of the phase velocity (its vanishing in particular), while the group velocity for such highly dispersive waves as the waves on vortices appears more relevant. Finally, both the critical state approach and the local stability approach cannot describe the formation of the stagnation point on the axis and, even more importantly, do not take into account the downstream boundary conditions. This makes these two approaches appear at least incomplete as it is well documented experimentally that (i) the vortex breakdown phenomenon is very sensitive to the streamwise boundary conditions and application of downstream suction, for instance, eliminates a breakdown structure [5, 7]; (ii) "the perturbations do not move away from the location where they had been generated, and oscillations are localized in space" [3]. We will comment on the last observation later and just note here that spatial localization of disturbances do not necessarily imply nonlinear effects but can be due to mean flow inhomogeneity. Spectral analysis of the experimental data [19, 20] indicates that the wake oscillations downstream of a breakdown structure have a single dominant frequency of less than 10 Hz. It was also shown that, once started, the oscillations continue after the source of disturbances was removed [21].

In this investigation we adopt a description in terms of linear instability waves propagating on a slowly varying mean flow. First we study the stability of the "parallel" Q-vortex [14] to show how the concept of zero group velocity comes into play and discuss the relevance of the concept of *global instability* [16-18] to the breakdown phenomenon. The detailed analysis of the global stability of a spatially evolving vortex will be the subject of future work. For the present parallel analysis we use a spatio-temporal approach which resolves, contrary to previous analyses which only considered temporal or spatial instability, the question of absolute or convective instability of the physical system by considering its impulse response [16, 17, 22, 23]. This is strongly supported by the experiments of Lambourne & Bryer [24] who found that disturbances in a swirling flow grow both in space and time. Intuitively, absolute and convective instability can be defined as follows: if a perturbation at any fixed location of the flow grows without bound (in the context of linear theory) for large times, the flow is absolutely unstable. If, on the other hand, a perturbation is convected away as it grows such that at large times all disturbances decay to zero at any fixed location, the flow is convectively unstable. This definition depends of course on the frame of reference but in applications there is always a distinguished frame of reference fixed relative to, say, a vortex generator or the apex of a delta wing where the delta-vortex originates.

We consider in the following a swirling flow with a mean velocity profile similar to a vortex trailing from a delta wing in an incompressible and inviscid fluid. In cylindrical coordinates (r, θ, z) it is described by the velocity vector $\underline{U}=(0, V(r), W(r))$ with the axial velocity $W(r)$ and swirl velocity $V(r)$ given in dimensionless form by

(1) $W(r) = W_0 + W_1 \exp(-r^{*2}); \quad V(r) = q \, [1-\exp(-r^{*2})] \, / \, r^*$.

Here r* is the radial distance normalized with the characteristic radius of the vortex core. A normal mode perturbation

(2) $(u', v', w') = [u(r), v(r), w(r)] \exp[i(kz - n\theta - \omega t)]$

is superimposed on the mean flow. It is governed by the Howard-Gupta equation

(3) $DSD*u - [1 + a/\gamma + b/\gamma^2]u = 0$,

where $D = d/dr$, $D* = D + 1/r$,

(4a, b) $S = r^2/(n^2 + k^2r^2)$, $\gamma = kW(r) - nV(r)/r - \omega$,

(4c) $a(r) = rD[(n^2 + k^2r^2)^{-1} (krD*V + nDW)]$,

(4d) $b(r) = -2kV(r) S [krD*V + nDW]$.

The boundary conditions are:

(5) $u(0) = 0$ if $n \neq 0$ and $Du(0) = 0$ if $n = 0$; $u \longrightarrow 0$ as $r \longrightarrow \infty$.

For large r the equation (3) reduces to

(6) $D(SD*u) - u = O$,

which has the solution (Lessen et al. [14])

(7a) $u(r) = C D[K_n(kr)]$.

The asymptotic behavior of (7) was used to implement the boundary condition at a finite large r=R, varying between 4 and 6 in our calculations, in the form

(7b) $Du/u (r=R) = D^2K_n(kR)/DK_n(kR)$.

Equation (3) can now be written in the form

(8) $d^2u/dr^2 + (1/r) P(r) du/dr + [(1/r^2) Q(r) + f(r)]u = 0$

where

$P(r) = (3n^2 + k^2r^2)(n^2 + k^2r^2)^{-1}$, $Q(r) = 2n/(n^2 + k^2r^2) - n^2 - k^2r^2 - 1$,

$f(r) = -a/(S\gamma) - b/(S\gamma^2)$.

Because both k and ω are complex, we do not have to worry about zeros of γ. It allows us to look for a solution in the form of a Frobenius series near the regular singularity at r=0. By expanding P(r), Q(r) and f(r) in power series one obtains a solution of the following form

(9) $u = r^{n-1} (a_0 + a_2r^2 + ...)$.

Starting with this expansion at r=0.01, the solution of (8) is advanced towards r=R by numerical integration and then matched to the known asymptotic solution (7b). The shooting method with a globally convergent multidimensional Newton-Raphson scheme [15] was used to find the eigenvalues. The code was tested by comparing with known eigenvalues for real k [14]. For the calculations the following parameters were chosen to match the experiments of Garg & Leibovich [19], noting that q is different from [19] because we use a different profile.

$$(19) \qquad W_0 = 18.0 \,, \quad W_1 = -13.0 \,, \quad q = -18.828 \,.$$

These parameters correspond to a distance 3.8 cm after the breakdown point (stagnation point). The calculations yield a saddle point of $\omega(k)$ in the complex k-plane at $k=0.823+0.372i$ with a complex frequency $\omega=2.593+0.427i$. Such a point with positive ω_i , together with the pinching requirement verified on fig. 1, indicates absolute instability.

This confirms the hypothesis that the oscillations developing on a breakdown structure are likely to be self-excited. Since we have assumed a mean flow that mimicks breakdown, our analysis can however not predict the onset of breakdown. Starting from the study of Tsai & Widnall [25] who argue that the observed disturbance buildup at the critical section of a divergent vortex apparatus should correspond to trapping of a wave with zero group velocity rather than phase velocity as in Benjamin and other recent criteria [26, 27], the following procedure is proposed for the future. The next step is clearly an analysis of a slowly varying mean flow. in a globally unstable case, an instability wave can move upstream from the turning point region of the slowly diverging problem [18] and the conceptual difficulties with a trapped wave as in [25] do not occur. At the same time, the global analysis [16-18, 28] can take downstream (and upstream) boundary conditions into account in a natural way.

References

[1]   P. Saffman, *Vortex Dynamics*. Cambridge Univ. Press, 1992.

[2]   D. Peckhman & S. Atkinson, Aeronautical Research Council, CP 508 (1957).

[3]   T. Sarpkaya, J. Fluid Mechanics, **4**, 545 (1971).

[4]   M. Hall, Ann. Rev. Fluid Mech., **4**, 195 (1972).

[5]   S. Leibovich, Ibid., **10**, 221 (1978).

[6]   M. Escudier, Prog. Aerospace Sci., **25**, 189 (1988).

[7]   J. Delery, Prog. Aerospace Sci., **30**, 1 (1994).

[8]   M. Lee & C.-M. Ho, Applied Mech. Reviews, **43**, 209 (1990).

[9]   Douady, Couder & Brachet, Phys. Rev. Letters, (1991).

[10]   A. Bers, in *Handbook of Plasma Physics* (M.N. Rosenbluth & R.Z. Sagdeev, Eds.), Vol. 1, Chap. 3.2., North Holland, 1983.

[11]   G. Batchelor, *An Introduction to Fluid Dynamics*, Chap. 7.5., Cambridge Univ. Press, 1970.

[12]   H. Squire, Imperial College of Science and Technology, Aeronautics Dept., Report N 102 (1960).

[13]   L. Howard & A. Gupta, J. Fluid Mech., **14**, 463 (1962).

[14]   M. Lessen, P. Singh & F. Paillet, J. Fluid Mech., **63**, 753 (1974).

[15]   W. Press et al., *Numerical Recipes in Fortran, The Art of Scientific Computing*, Cambridge Univ. Press, 1992.

[16]   J.-M. Chomaz, P. Huerre & L. Redekopp, Phys. Rev. Letters, **60**, 25 (1988).

[17]   P. Monkewitz, Eur. J. Mech. B/Fluids, **9**, 395 (1990).

[18]   P. Huerre & P. Monkewitz, Ann Rev. Fluid Mech., **22**, 473 (1990).

[19]   A. Garg & S. Leibovich, Phys. Fluids, **22**, 2053 (1979).

[20]   I. Gursul, AIAA J., **32**, 225 (1994).

[21]   R. Chanaud, J. Fluid Mech., **21**, 111 (1965).

[22]   D. Bechert, Z. Flugwiss. Weltraumforsch., **9**, 356 (1985).

[23]   P. Monkewitz, P. Huerre & J.-M. Chomaz, J. Fluid Mech., **251**, 1 (1993).

[24]   N. Lambourne & D. Bryer, Aeronautical Research Council, R&M 3282, 1961.

[25]   C. Tsai & S. Widnall, Phys. Fluids, **23**, 864 (1980).

[26]   G. Brown & Lopez, J. Fluid Mech. (1988).

[27]   R. Spall, T. Gatski & C. Grosch, Physics of Fluids, **30**, 3434 (1987).

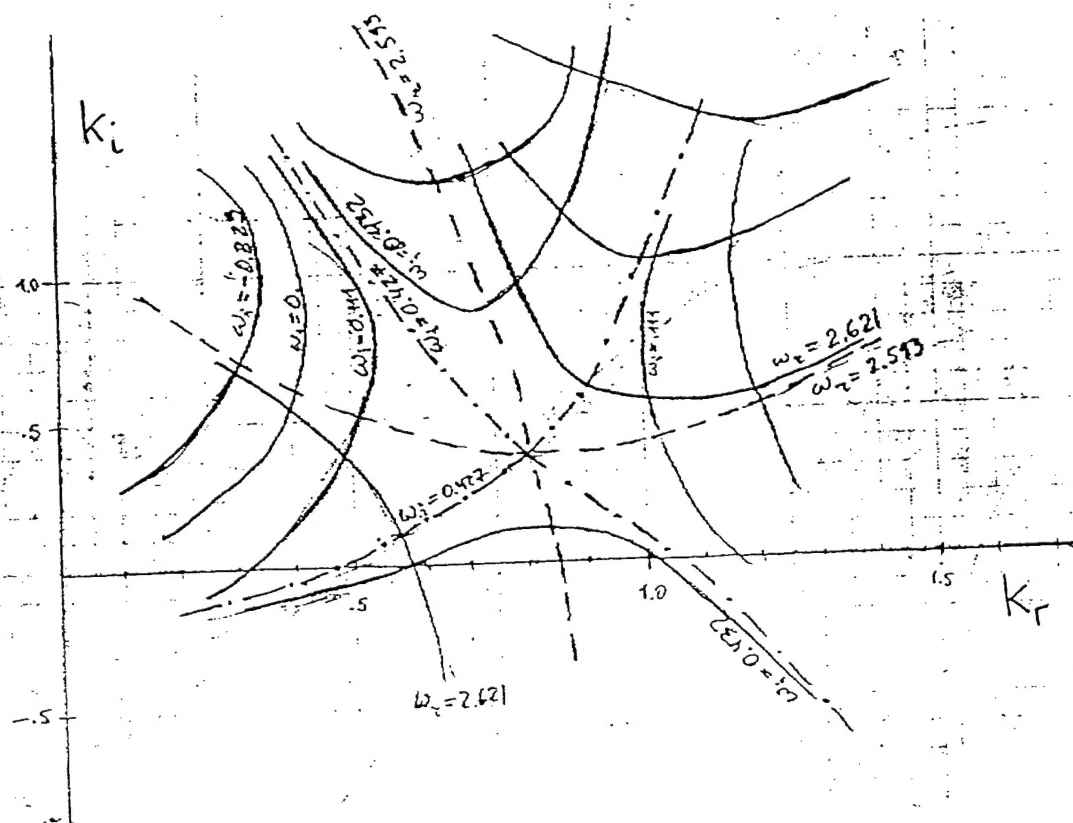[28]   M. Pesenson & P. Monkewitz, Phys. Rev. Letters, **70**, 2722 (1993).

Fig. 1 Saddle- and pinchpoint in the complex k-plane for n=-1 mode.